MAGYAR ÁLLAMI
EÖTVÖS LORÁND
GEOFIZIKAI INTÉZET

GEOFIZIKAI
KÖZLEMÉNYEK

ВЕНГЕРСКИЙ
ГЕОФИЗИЧЕСКИЙ
ИНСТИТУТ
ИМ Л. ЭТВЕША

ГЕОФИЗИЧЕСКИЙ
БЮЛЛЕТЕНЬ

# GEOPHYSICAL

## TRANSACTIONS

EÖTVÖS LORÁND GEOPHYSICAL INSTITUTE OF HUNGARY

CONTENTS


| | | |
|---|---|---|
| Velocity estimation by zero-offset migration in a layered medium | *E. Maeland* | 3 |
| Integrating chemical and physical logging data; examples from the Ocean Drilling Program | *M. A. Lovell, P. K. Harvey, R. Pelling, J. F. Bristow* | 19 |
| Relationship of porosity and permeability to mercury injection derived parameters for sandstones of the Törtel Formation, Hungary | *A. M. A. El-Sayed* | 35 |
| Analysis of gravity anomalies due to cylinrical structures with linearly varying density | *A. V. Varaprasada Rao, G. Sahadev, P. Srinivasa Rao, N. Sundararajan* | 47 |
| Interpretation problems of electric sounding and profiling in regions of complicated geology and rugged terrain | *A. Frasëri* | 55 |


VOL. 38. NO. 1. JUNE 1993. (ISSN 0016-7177)

BUDAPEST

TARTALOMJEGYZÉK


| | | |
|---|---|---|
| Sebességbecslés rétegzett közegben időszelvény migrációval | *E. Maeland* | 18 |
| A kémiai és fizikai karotázs adatok integrálása; példák az óceáni mélyfúrási programból | *M. A. Lovell, P. K. Harvey, R. Pelling, J. F. Bristow* | 32 |
| Porozitás és permeabilitás kapcsolata higanyinjektálásból származtatott paraméterekkel, a Törtel formáció homokköveire | *A. M. A. El-Sayed* | 45 |
| Lineárisan változó sűrűségű hengeres szerkezetek gravitációs anomáliáinak vizsgálata | *A. V. Varaprasada Rao, G. Sahadev, P. Srinivasa Rao, N. Sundararajan* | 53 |
| Elektromos szondázás és szelvényezés értelmezési problémái bonyolult földtani szerkezetű és egyenetlen felszínű területeken | *A. Frasëri* | 65 |


СОДЕРЖАНИЕ


| | | |
|---|---|---|
| Оценка скорости в слоистом разрезе с помощью миграции временного разреза | *Э. Мэйланд* | 18 |
| Интеграция данных химичуского и физического каротажа, примеры скважин на океане | *М. А. Повелл, П. К. Хервей, Р. Пеллинг, Дж. Ф. Бристоу* | 32 |
| Связь пористости и проницаемости с параметрами, выведенными по нагнетанию ртути, для песчаников тертельской формации | *А. М. А. Эль-Саед* | 46 |
| Исследование аномалий силы тяжести от цилиндрических структур при линейно изменяющейся плотности | *А. В. Варапрасада Рао, Г. Сахадев, П. Сриниваса Рао, Н. Сундарараджан* | 53 |
| Проблемы интерпретации данных электрического зондирования и профилирования на стках, характеризующихся со сложным геологическим строением и неровностью рэльефа | *А. Фрашери* | 66 |

# The proven technology to help you reduce risk and increase your success rate – worldwide.

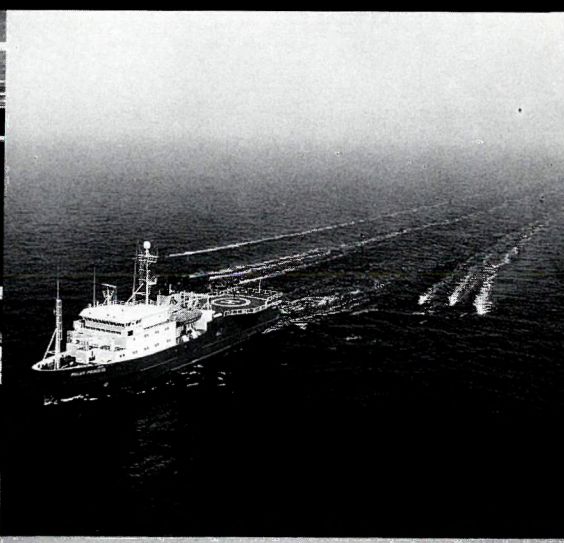

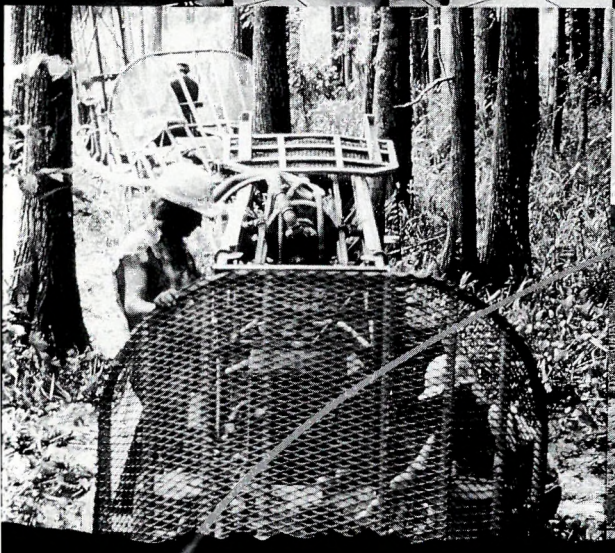

HGS

## Halliburton Geophysical Services

6909 Southwest Freeway Houston, TX 77074 Ph: (713) 774-7561 FAX: (713) 778-3487/Telex: 76-2781

A Halliburton Company

# *DON'T BUY EQUIPMENT OR SERVICES UNTIL YOU KNOW THE FACTS*

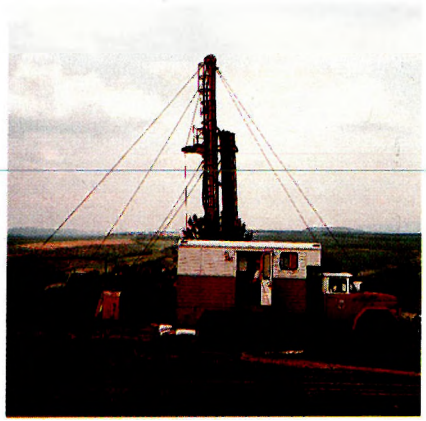

ELGI's Well Logging Divison has put its 25 years of experience to work again in the new line of well logging technology in

water,

coal,

mineral,

geotechnical

prospecting

## HERE'S WHAT WE OFFER

- Complete series of surface instruments from portable models to the PC controlled data logger
- Sondes for all methods: electrical, nuclear, acoustic, magnetic, mechanical, etc.
- Depth capacity down to 5000 m
- On-site or office computer evaluation
- International Metrological Base for calibration to true petrophysical parameters
- Training and in-house courses
- Design laboratory for custom-tailored assemblies

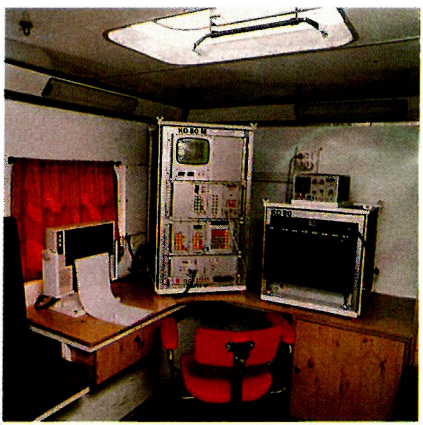

Just think of us as the scientific source of borehole geophysics you may never have heard of

SALES ✣ ✣ ✣ ✣ RENTALS ✣ ✣ ✣ ✣ SERVICES

**Well Logging Division of ELGI**
**POB 35, Budapest, H-1440 Hungary**
**Phone: (361) 252-4999, Telex: 22-6194,**
**Fax: (361) 183-7316**

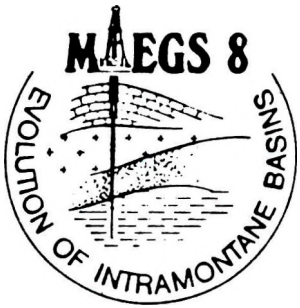


# 8th Meeting of the Association of European Geological Societies

Topic:
EVOLUTION
OF INTRAMONTANE BASINS
ON THE EXAMPLE OF THE PANNONIAN BASIN WITH PARTICULAR EMPHASIS
ON SEQUENCE STRATIGRAPHY AND NEOTECTONICS

Schedule:

| | | |
|---|---|---|
| September | 18 (Sat) | |
| | 19-20 (Sun-Mon) | (A) Pre-Meeting Field Trip:<br>Marginal Facies of the Pannonian Basin (including lignite deposits) |
| | 21 (Tue) | Registration and Sightseeing in Budapest,<br>with a visit to the Hungarian Geological Survey (founded in 1869) |
| | 22-24 (Wed-Fri) | Technical Sessions (including a Poster Session) |
| | 25-26 (Sat-Sun) | Post-Meeting Field Trips:<br>(B) Geology, agriculture, environment and urban engineering.<br>Geology in the Pannonian Basin.<br>(C) Oil and gas, underground water, and geothermy in the Pannonian Basin. |

Language: English

During the Meeting,
an All-European Regional Meeting of the International Geological Correlation Programme (IGCP)
will also be held

Address:
MAEGS-8 Org. Com.
Hungarian Geological Society
H-1027 Budapest, Fő u. 68. I. 102.
Hungary

Telephone: 36-1-251-0999; 36 - 1- 251 - 0089 / I. VETŐ
Telex: 61- 225220 ( máfi h )
Telefax: 36 - 1 - 251 - 0703

# ESS - 03 - 24

## PC based 24 channel portable seismograph

ESS-03 was designed for high-resolution subsurface imaging using up-to-date electronics and computer technology. Compared with excavation or dense drilling networks, it offers a highly cost-effective solution for geotechnical problems.

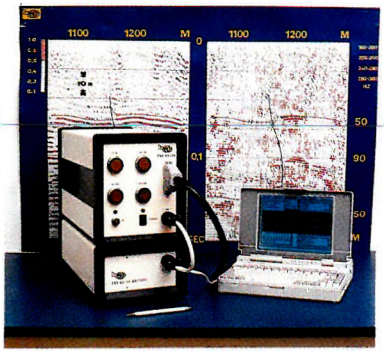


It is an excellent tool

- for raw material prospecting;
- for determining static corrections for surface seismic methods;
- for acquiring information when designing large scale foundations such as factories, dams or roads;
- for seismic investigation of well-sites;
- for in-mine exploration;
- for detection of destructive building-vibrations.

ESS-03 can be used not only for rapid and inexpensive data acquisition, but the built-in PC and software package offer excellent on-site processing, quick-look interpretation, and visual display of the results.

*Founded in 1919*

### Specifications:

Frequency response: 1-8000 Hz
Resolution: 12 bit A/D+42 dB IFP
Built-in electronic roll along switch
Microprocessor control 80386-SX-20
Data recording on floppy disc 1.44 MB, hard disc 80 MB
Menu-driven operating commands
LCD display with VGA resolution
Self-testing programs and parameter checking
Weight: 10 kg
Dimensions: 200*220*450 mm

**Eötvös Loránd Geophysical Institute of Hungary**

Budapest, XIV. Columbus u. 17-23.
Letters: H-1440 Budapest, POB. 35.
Phone: (36-1) 184-3309
Fax:(36-1) 163-7256
Telex: (61) 22-6194 elgi h
E-mail: H6123 TIT@ELLA.HU

GEOPHYSICAL TRANSACTIONS 1993
Vol. 38. No. 1. pp. 3-18

# VELOCITY ESTIMATION BY ZERO-OFFSET MIGRATION IN A LAYERED MEDIUM

Einar MAELAND*

Migration of seismic data from buried point diffractors in a 2-D medium with plane dipping reflectors is used to estimate a velocity macro-model. The surface data are extrapolated with a known velocity to a new reference level by wave equation datuming, followed by zero-offset migration with the constant velocity at the new datum. The diffracted energy will then be out of focus, so the imaging condition is modified to allow for an extra time-shift. If the diffracted energy focuses, the position of this focus and the extra time-shift determines the velocity in the next layer. Examples on synthetic data illustrate the quality of the analysis.

**Keywords: migration, geometrical optics, caustics, image, time-shift, diffractions, radius of curvature**

## 1. Introduction

Migration of seismic reflection data consists of downward extrapolation of surface data, and imaging at a time when the downward wave is time-coincident with the upgoing wave [CLAERBOUT 1971]. If the velocity is in error, the 'image' will be out of focus. Among the algorithms designed to estimate velocity, depth focusing analysis generates displays that are similar to conventional velocity analysis. Several studies, including those of DOHERTY and CLAERBOUT [1976], YILMAZ and CHAMBERS [1984], FAYE and JEANNOT [1986], report the focusing aspects of migration. When migration is performed with erroneous velocity the zero-time image condition does not produce the best-focused data. However, if the imaged data at non-zero times are saved, a better velocity estimate may be obtained by interpreting the migrated output.

* Seismological Observatory, University of Bergen, Allegt. 41, N-5007 Bergen, Norway

Manuscript received: 13 March, 1992

In order to introduce approximate image formation, it is helpful to consider a physical model for which the problem can be solved analytically. Consider a layered medium containing plane dipping reflectors, with a constant velocity in each layer. Assume that the surface data have been extrapolated to a new reference level by wave equation datuming [BERRYHILL 1979]. The objective is to find the position of a point diffractor and the velocity within the next deeper layer. The analysis can then, without loss of generality, be confined to a model with two contiguous layers.

It is possible to estimate velocities by trial and error, until the diffracted energy comes into focus. This can be done by keeping the imaging condition fixed while the velocity is given different values or, which is more reasonable, to choose one velocity but relax the imaging condition to allow for an extra time-shift. In general, if the imaging condition is modified, the result will be an image which may be rather complicated to describe algebraically. However, it is possible to extract one particular (erroneous) velocity that yields an image which is representative of the entire family of images.

The aim of this paper is to present an analysis based on wave equation datuming and velocity determination by migration. The principal steps include (i) obtaining an initial estimate of the velocity field which is used to perform the depth migration, and (ii) interpretation of the focusing errors and using them to estimate the velocity in the next lower layer. The proposed technique does not require modification of existing extrapolation algorithms.

## 2. Formulation of the problem

Assume that a single point diffractor is buried in the lower layer of a two-layer medium. For simplicity, but with no loss of generality, the problem will be treated as two dimensional. Let $(x, z)$ be cartesian coordinates, with $x$ and $z$ in the horizontal and vertical directions, respectively. Let the boundary dividing the two layers be a plane, dipping surface defined by

$$z = z_0 - \tan(\alpha)\, x \ , \tag{1}$$

where $\alpha$ is the dip-angle. The position of the point diffractor is $S = (x_*, z_*)$. It is convenient to use relative coordinates $(\xi, \eta)$, with the origin at $(0, z_0)$ and rotation angle $\alpha$. Hence, the $\xi$-axis is along, and the $\eta$-axis is normal to the plane surface Eq. (1). The transformation from $(x, z)$ to $(\xi, \eta)$ is given by

$$\begin{aligned} \xi &= -(z - z_0)\sin(\alpha) + x\cos(\alpha) \ , \\ \eta &= (z - z_0)\cos(\alpha) + x\sin(\alpha) \ . \end{aligned} \tag{2}$$

The position of the diffractor in the rotated coordinates will be denoted by $(\xi_*, \eta_*)$. Since $\eta_* > 0$, then $z_* > [z_0 - \tan(\alpha)\, x_*]$.

Consider a plane, refracting surface ($g$) separating two media with velocities $c_1$ (above) and $c_2$ (below). A point source ($S$) is the common centre of a family of concentric spherical wavefronts. Two cases are of interest, viz., $c_1 < c_2$ and $c_1 > c_2$, which are displayed in *Figs. 1A* and *1B*, respectively. A ray from source $S$ strikes the surface $g$ at an angle of incidence $\beta_2$ (which is measured relative to the $\eta$-axis). The angle of refraction, $\beta_1$, is given by Snell's law

$$\sin(\beta_1) / c_1 = \sin(\beta_2) / c_2 \,. \qquad (3)$$

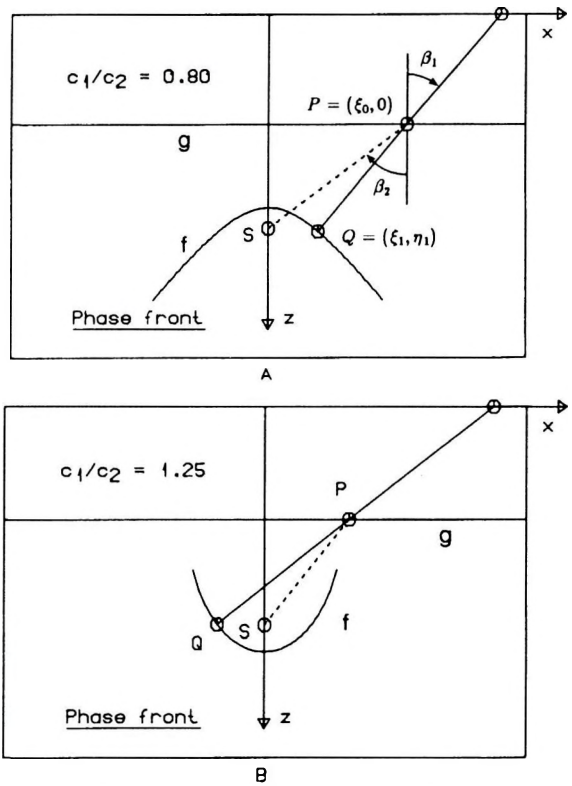


*Fig. 1.* Construction of zero-distance phase front of refraction ($f$), A— $\gamma<1$; B—$\gamma>1$ ($\gamma = c_1/c_2$). Rays are refracted at point $P$, and continued to a point $Q$ such that $QP = \gamma\, SP$
$g$—refracting surface; $c_1$—velocity above and $c_2$— velocity below the refracting surface; $S$—a point source

*1. ábra.* A hullámtörés $t(0)$ fázisú frontjának ($f$) szerkesztése. A—$\gamma<1$; B— $\gamma>1$ ($\gamma = c_1/c_2$). A sugarak megtörnek a $P$ pontnál és folytatódnak a $Q$ pontig oly módon, hogy $QP = \gamma\, SP$.
$g$—törési felület; $c_1$—a törési felület feletti és $c_2$—alatti sebességek; $S$—pontforrás

*Рис. 1.* Составление фронта $f$ преломления волны при фазе $t(0)$. А— $\gamma<1$; В—$\gamma>1$ ($\gamma = c_1/c_2$). Лучи преломляются на точке $P$ и продолжаются до точки $Q$ при $QP = \gamma\, SP$.
$g$—преломляющая поверхность; $c_1$ и $c_2$—скорости над преломляющей поверхностью и под ней; $S$—точечный источник

Let $P = (\xi_0, 0)$ be a point on the refractor, and $SP = c_2 t_0$, where $t_0$ is the traveltime from source $S$ to point $P$. Then,

$$\sin(\beta_2) = (\xi_0 - \xi_*) / c_2 t_0 . \tag{4}$$

Let the refracted ray be continued to a point $Q = (\xi_1, \eta_1)$, such that $QP = (c_1/c_2)\, SP$. As point $P$ moves over surface $g$, the points $Q$ will all lie on a surface $f$. This surface is defined as the zero-distance phase front of refraction [CORNBLEET 1984]. If $SP = c_2 t_0$, it follows that $QP = c_1 t_0$, and

$$\sin(\beta_1) = (\xi_0 - \xi_1) / c_1 t_0 ,$$
$$\cos(\beta_1) = \eta_1 / c_1 t_0 . \tag{5}$$

Thus, a set of parametric equations are obtained

$$\xi_1 - \xi_* = c_2 t_0 (1 - \gamma^2) \sin(\beta_1) / \gamma ,$$
$$\eta_1 = \gamma\, c_2 t_0 \cos(\beta_1) , \tag{6}$$

where $\gamma = c_1/c_2$ is the velocity ratio. If the parameter $\beta_1$ is eliminated, the result is, by means of the relation $\cos(\beta_2) = \eta_*/c_2 t_0$, that the zero-distance phase front is given by

$$(\xi_1 - \xi_*)^2/(\gamma^2 - 1) + (\eta_1/\gamma)^2 = \eta_*^2 . \tag{7}$$

Hence, the zero-distance phase front is an ellipse or a hyperbola depending on whether $\gamma > 1$ or $\gamma < 1$, respectively. The conclusion is that kinematic migration of zero-offset data with the constant velocity $c_1$ yields the zero-distance phase front.

For velocity ratios ($\gamma$) of 0.8 and 1.25, respectively, ray paths from the point diffractor to the receiver positions on the $x$-axis are shown in *Figs. 2A* and *2B*; the corresponding refracted rays and the zero-distance phase front are in *Figs. 3A* and *3B*.

## 3. Focusing analysis

If data from a single point diffractor in a homogeneous medium are considered, migration with erroneous velocity yields an image that is a phase front of zero distance. Consider two layers where the velocities of wave propagation are $c_1$ and $c_2$, respectively. Rays from a point source in the deeper layer will be collimated to parallel rays by refraction at a hyperbolic surface if $\gamma < 1$, or an elliptic surface if $\gamma > 1$. The hyperbolic or elliptical refractor produces a plane phase front, whereas a plane refractor gives a hyperbolic or elliptical phase front for $\gamma < 1$ or $\gamma > 1$, respectively [CORNBLEET 1984]. Based upon this observation, if the dip-angle ($\alpha$) is given for a plane interface, the

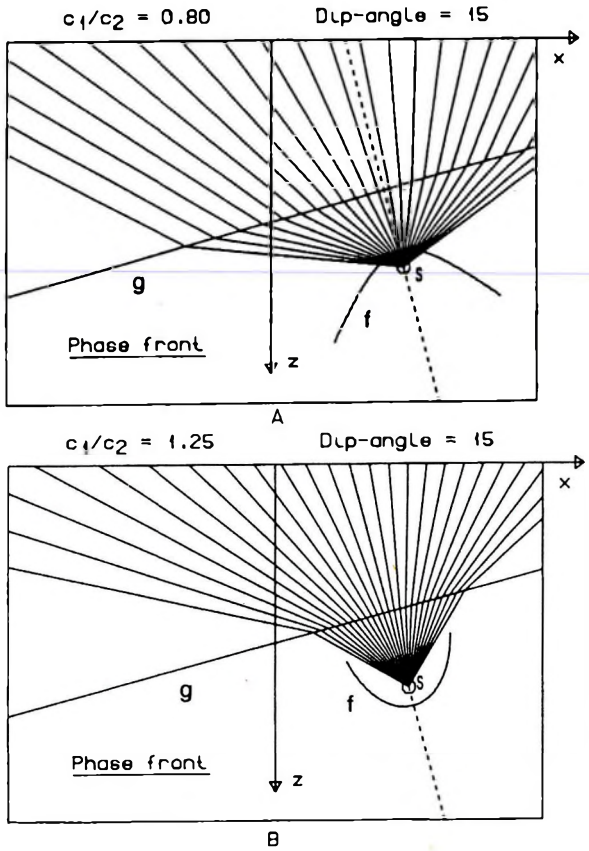


*Fig. 2.* Ray paths from source (*S*) to points on the x-axis when A— $\gamma < 1$, and B— $\gamma > 1$. (exp. see Fig. 1)

*2. ábra.* Sugárutak a forrásponttól (*S*) az x-tengely pontjaiig A— $\gamma < 1$, és B— $\gamma > 1$ esetén. (jelmagyarázat: lásd 1. ábra)

*Рис. 2.* Лучи от источника (*S*) до оси x, A–для случая $\gamma < 1$, B–при $\gamma > 1$. (условные обозначения см. на Рис.1 )

velocity ($c_2$) in the lower layer may be determined by migration with the velocity ($c_1$) in the upper layer.

Making use of the exploding reflector concept, consider any wavefront with centre at $S = (x_*, z_*)$ at time $t_1 \neq 0$; i.e., a spherical wave with radius $c_2 t_1$. In order to perform reliable focusing analysis, a parallel phase front at a distance $(t_1 + c_1 \Delta t)$ must be calculated, and then choose $\Delta t$ so that the diffracted energy (eventually) comes to a focus. However, if the velocity is in error, perfect focus cannot be attained. Associated with a phase front are the corresponding families of rays. A wave field corresponds to a family of rays that can, and usually does, exhibit a property that does not reside in any of the individual rays, namely

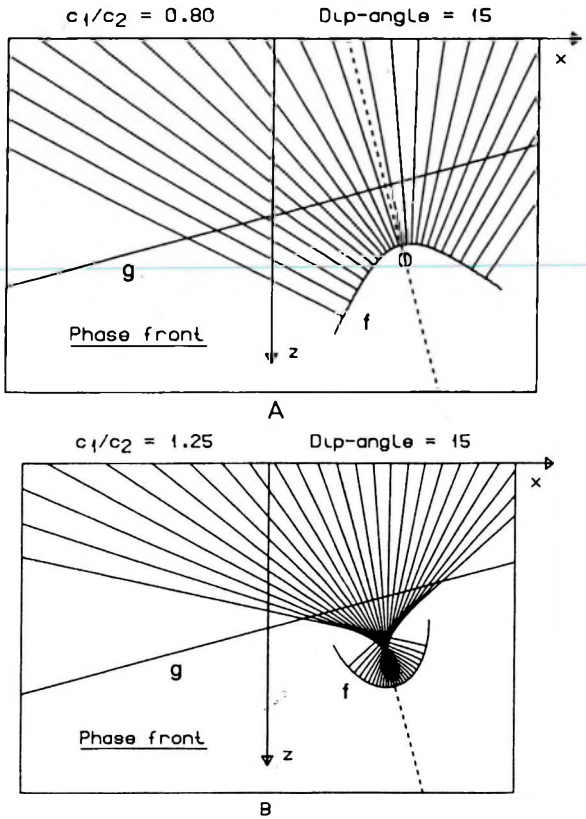


*Fig. 3.* Ray paths from zero-distance phase front of refraction when A— $\gamma<1$, and B— $\gamma>1$ (exp. see Fig. 1)

*3. ábra.* Sugárutak a hullámtörés $t(0)$ fázisfrontjától A—$\gamma<1$ ,és B— $\gamma>1$ estén (jelmagyarázat: lásd 1. ábra)

*Рис. 3.* Лучи от фронта преломления при фазе $t(0)$ А–для случая $\gamma<1$, В–для $\gamma>1$. (условные обозначения см. на Рис. 1)

focusing. This occurs on the envelope of neighbouring rays (caustics). Wave fields are dominated by caustics, which form the significant structure of images formed by migration of seismic data. The caustic represents the concentration of energy, or the 'aberrated image' of the point source. If the caustic is cusped (two branches of the curve meet), then exceptional, high amplitudes may be expected, and the cusp replaces the exact focus which exists when $\gamma = 1$.

Given a parallel phase front, it is possible to examine whether the phase front will develop a cusp at a certain time $\Delta t \neq 0$. Points at which this occurs are points at which adjacent rays intersect. The locus of all such points is a caustic. A parallel phase front is defined by $\xi = \xi(t)$ and $\eta = \eta(t)$, where

$$\xi(t) = \xi_1 + c_1 t \sin(\beta_1) \quad ,$$
$$\eta(t) = \eta_1 - c_1 t \cos(\beta_1) \quad . \tag{8}$$

A positive time ($t > 0$) indicates that the phase front is moving toward negative $\eta$-values. Due to the symmetry about $\xi = \xi_*$, it is sufficient to describe the phase front in the vicinity of this line, i.e., small angles $\beta_1$; hence

$$\xi(t) - \xi_* = [\, c_1 t + \eta_* (1 - \gamma^2)/\gamma \,]\ \beta_1 + \ldots$$
$$\eta(t) = \gamma \eta_* - c_1 t + \frac{1}{2} [\xi(t) - \xi_*]\ \beta_1 + \ldots \tag{9}$$

The radius of curvature given by

$$R(t) \approx \partial \xi(t)/\partial \beta_1 = c_1 t + (1-\gamma^2)\, \eta_*/\gamma + \ldots \tag{10}$$

is equal to zero at a time

$$c_1 \Delta t = (\gamma^2 - 1)\, \eta_*/\gamma = -R(0) \quad . \tag{11}$$

In other words, the phase front is cusped [MAELAND 1989] and due to the symmetry, the position of the cusp of the caustic is $(\xi_C, \eta_C) = (\xi_*, \eta_*/\gamma)$. The caustic and the cusp can be identified in Fig. 3B; in Fig. 3A, they can be identified only if the rays are extended below the phase front.

Data transfer to the floating datum (reference level) is performed by time-shifting every seismic trace by an amount defined by the difference in elevation and a known or an estimated velocity model. Although an extra time-shift can smear seismic energy and deteriorate spatial resolution on the depth section, the result may well be another 'focus'. The position $(\xi_C, \eta_C)$ is relative to the rotated coordinate system, so

$$\eta_C = (z_C - z_0) \cos(\alpha) + x_C \sin(\alpha) \quad . \tag{12}$$

The position $(z_0)$ and the dip-angle $(\alpha)$ are given by zero-offset migration with $\Delta t = 0$. Then, solving equation (11) for the velocity ratio

$$\gamma^2 = 1 + c_1 \Delta t / \eta_C \quad . \tag{13}$$

In this formula velocity $c_1$ is known whereas the time-shift $(\Delta t)$ and the position of the focus must be determined by inspection of the migrated output.

## 4. Illustrative examples

In order to indicate the quality of the focus when the imaging condition is modified, migration is executed by the phase-shift operator [GAZDAG 1978], but allowing for an extra time-shift in the imaging condition. The input signal

is a zero-phase Ricker wavelet, i.e., the second-derivative of $f(t) = \exp[-2(t/T)^2]$, where $T = 0.05$ sec. The velocity in the upper layer is $c_1 = 1$ km/s, moreover, $z_0 = 1.0$ km and $\alpha = 15°$. A point diffractor is located at $x_* = 2$ km and $z_* = 1.0$ km. Finally, the extrapolation step is $\Delta z = 0.01$ km.

The synthetic zero-offset section is displayed in *Fig. 4A* when $\gamma < 1$. *Figures 4B* and *4C* contain the migrated results while the imaging condition is applied at $t = 0$ and $t = \Delta t$, respectively. The corresponding results when $\gamma > 1$ are displayed in *Figs. 5A*, *5B* and *5C*, respectively. According to the proposed strategy, when the imaging condition is modified ($\Delta t \neq 0$), the dip of the reflector is the same, but its position will change, cf., Figs. 4C and 5C, respectively. The true position of the reflector is indicated by the sloping line, and the position of the aberrated focus ($\eta_C$) must be measured relative to this line. The quality of the focus depends on the aperture, so the quality when $\gamma > 1$, is much better than when $\gamma < 1$. Moreover, the net phase-shift of approximately $\pi/2$ when the parallel phase front passes through the cusp of the caustic may be used to decide whether a focus is in sight or not. The change in sign of the curvature of the phase front may also be useful. A drawback is that artifacts caused by phase wrapping may be strongly in evidence, cf., Fig. 5C. Phase wrapping is a consequence of the actual migration algorithm (the phase-shift method). No attempts have been made to avoid phase wrapping. The phase-shift operator was chosen to illustrate that migration need not be done with the most sophisticated of algorithms: as a matter of fact, any conventional migration algorithm may be used.

To summarize: if $\gamma < 1$, then $\Delta t < 0$, so imaging at time equal to $t = 0$ is too early (undermigration); if $\gamma > 1$, then $\Delta t > 0$ and the imaging principle is applied too late (overmigration). Migration with a velocity too small leaves the data in positive time and migration with a too large velocity pushes the data into negative time [MAELAND 1989].

## 5. Paraxial approximation

Given a plane dipping interface, it has been demonstrated that information from the zero-distance phase front can be used to estimate the velocity in a two-layer model. In principle, this is also true for a general interface; in fact, given the position of a refractor, it is possible to obtain an expression for the zero-distance phase front [CORNBLEET 1984]. However, the analysis is rather complicated algebraically, and soon becomes unwieldy, so this case is rarely treated mathematically until certain simplifying conditions are imposed. If only rays that are close to the $\xi$-axis are to be considered (paraxial approximation), nonspherical surfaces can usually be adequately represented by spherical approximations.

The imaging that occurs during the migration of seismic data is similar to the focusing of light by a lens. The focal-length of the 'lens' is determined by

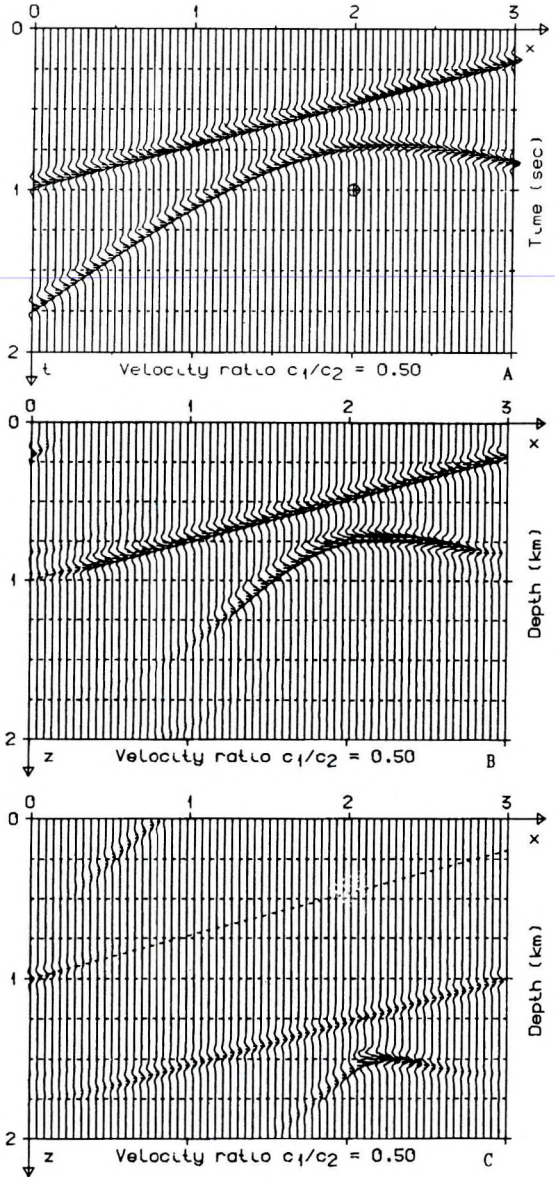


*Fig. 4.* A—Synthetic zero-offset sections when $\gamma = 0.5$; B— migration and imaging when $t = 0$ and C—when $t = \Delta t$

*4. ábra.* A—Szintetikus $t(0)$ szelvények $\gamma = 0{,}5$ esetén; B—migráció és leképezés $t = 0$ és C—$t = \Delta t$ esetén

*Рис. 4.* А—Синтетический разрез $t$ (0) при $\gamma = 0{,}5$; В—миграция и отображение $t = 0$; С—миграция и отображение $t = \Delta t$

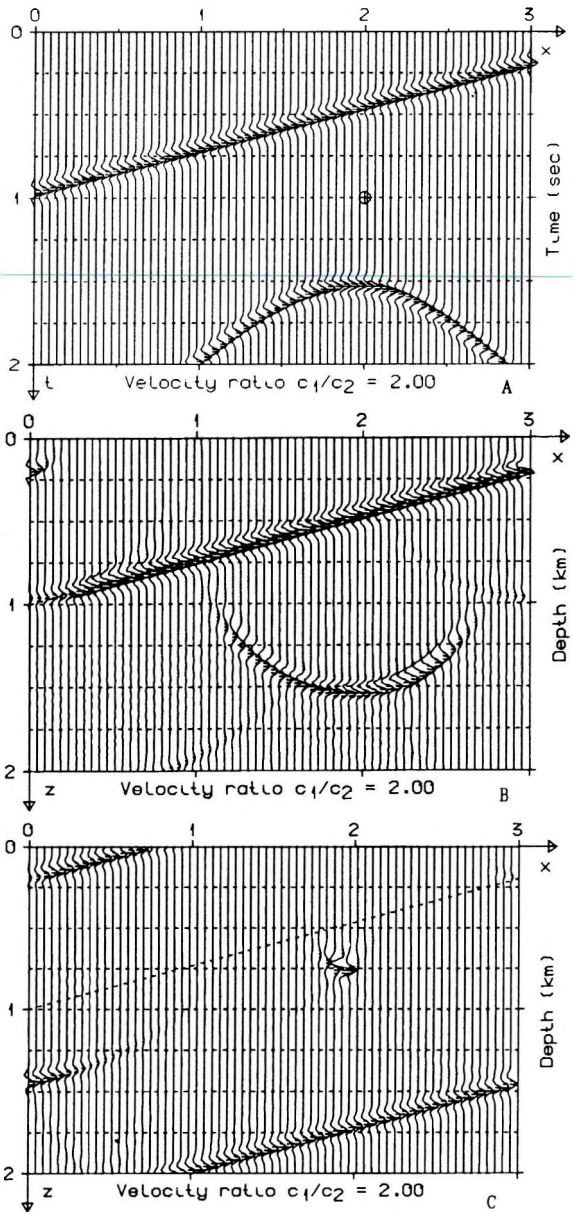


*Fig. 5.* A—Synthetic zero-offset section when $\gamma = 2.0$; B—migration and imaging when $t = 0$ and C—when $t = \Delta t$

*5. ábra.* A—Szintetikus $t$ (0) szelvények $\gamma = 2{,}0$ esetén; B— migráció és leképezés $t = 0$ és C—$t = \Delta t$ esetén

*Рис. 5.* А—Синтетический разрез $t(0)$ при $\gamma = 2{,}0$; В—миграция и отображение $t = 0$, С—миграция и отовражение $t = \Delta t$

the velocity field, and a 'best-focused' image is made by changing the imaging condition. In the terminology of geometrical optics, distance $\eta_*$ is the object distance, distance $\eta_C$ is the image distance. In general, image distances are not the same for all rays, which means that the rays do not come to a single focus. This is a common feature of any reflecting or refracting surface and is known as wave-front aberration in the (optical) literature.

With a circular refractor of radius $r$, say, the analysis becomes more tractable. If the origin of the circle is located at $\xi=\xi_*$ and $\eta=r$, the lens equation [BORN, WOLF 1980] yields

$$1/\eta_C - \gamma/\eta_* = (1-\gamma)/r \,. \tag{14}$$

The sign convention is (relative to the positive direction of the $\eta$-axis) that a concave surface is characterized by $r > 0$, and a convex surface by $r < 0$. The focal length is the image distance for parallel incoming rays ($\eta_* \rightarrow \infty$); hence, $1/f = (1-\gamma)/r$. If the refractor is plane ($r \rightarrow \infty$), which is the case studied so far, the lens equation (14) reduces to $c_1\eta_C = c_2\eta_*$, so that the product of migration velocity and focusing depth equals the product of real medium velocity and real diffractor depth. The same relation was given by FAYE and JEANNOT [1986], although it was derived from a completely different type of argument.

Zero-offset migration yields the zero-distance phase front, with an apex located at $\eta_A = \gamma\eta_*$. Assuming that the paraxial approximation (rays close to the $\xi$-axis) is valid with symmetry about the line $\xi = \xi_*$, the position of the cusp of the caustic is $\eta_C = \eta_A + R_A$, where $R_A$ is the radius of curvature at the apex of the zero-distance phase front. The radius of curvature (which is positive if the direction from the apex of the zero-distance phase front to its centre of curvature is positive) can be computed by means of Eq. (14)

$$R_A = \eta_*(1-\gamma)\,\frac{(1+\gamma) - \gamma\eta_*/r}{\gamma+(1-\gamma)\,\eta_*/r} \,, \tag{15}$$

which is a function of $\gamma$, $\eta_*$ and $r$. Some extreme cases are

$$\begin{aligned} R_A &= 0 && \text{when} \quad r = \gamma\eta_*/(\gamma+1) \,, \\ R_A &= (1-\gamma^2)\,\eta_*/\gamma && \text{if} \quad r \rightarrow \infty \,, \\ R_A &= \infty && \text{when} \quad r = (\gamma-1)\,\eta_*/\gamma \,. \end{aligned} \tag{16}$$

Another interesting case is $r = \eta_*$, where $\eta_C = \eta_*$ and $R_A = \eta_*(1-\gamma)$. In this case, the zero-distance phase front is a circle, with its centre at the diffracting point position. Hence, a perfect focus exists at $\eta_*$. Moreover, if the refracting surface is plane ($r = \infty$), the focus (in the analytical geometry sense) of the zero-distance phase front is located at the true diffracting position. The con-

clusion is that focusing analysis is still possible, although the position of the cusp of the caustic may not always be accessible, e.g., when the radius of curvature at the apex of the zero-distance phase front becomes very large. This is always true since $\eta_C = \eta_A + R_A$; in which case $\eta_C \to \infty$.

## 6. Location of the image

With the sign convention that if time increases, the wave front moves to negative $\eta$-values, it follows that

$$c_1 \Delta t = -R_A = \eta_A - \eta_C \quad . \tag{17}$$

Since $R_A$ is given in terms of $\eta_*$ (the unknown position of the point diffractor), it is helpful to express it by the distance $\eta_C$ (the observed position of the cusp). From Eq. (14)

$$R_A = \eta_C (1-\gamma) \frac{(1+\gamma) - \eta_C/r}{1-(1-\gamma)\eta_C/r} \quad . \tag{18}$$

When $r \to \infty$, this yields $c_1 \Delta t = (\gamma^2 - 1)\eta_C$, which is in accordance with Eq. (11). In general, however, the relation between the parameters $\eta_C$, $\gamma$ and $\Delta t$ is not very informative, but the most important information can be obtained by means of figures.

The radius of curvature as a function of the velocity ratio is displayed in *Figs. 6A* and *6B* when $r > 0$ and $r < 0$, respectively. The dashed curve represents $r \to \infty$, in which case the radius of curvature will be denoted by $R_0 = R_A$ $(r = \infty)$. In Fig. 6a the position of the diffractor is fixed, in Fig. 6B the position of the cusp is fixed (when $r = \pm 3$ km). Perfect focus can be attained only if $R_A = 0$; hence, $r > 0$ implies focusing, which yields $|R_A| < |R_0|$, and vice versa when $r < 0$. Finally, in terms of the focal length $(f)$, the result is

$$R_A = \eta_* \frac{1-\gamma^2-\gamma\eta_*/f}{\gamma+\eta_*/f} \quad . \tag{19}$$

Hence, when $f > 0$ then $|R_A| < |R_0|$, and vice versa.

In general the centre of the circle will not be at $\xi = \xi_*$. Assume that the cusp has been observed at $\xi_C \neq \xi_*$, with a corresponding point diffractor at $\xi_D \neq \xi_*$. In the terminology of geometrical optics [BORN, WOLF 1980], the ratio of the height $\xi_C - \xi_*$ of the image to the height $\xi_D - \xi_*$ of the object is the magnification

$$m = (\xi_C - \xi_*)/(\xi_D - \xi_*) = \gamma\eta_C/\eta_* \quad . \tag{20}$$

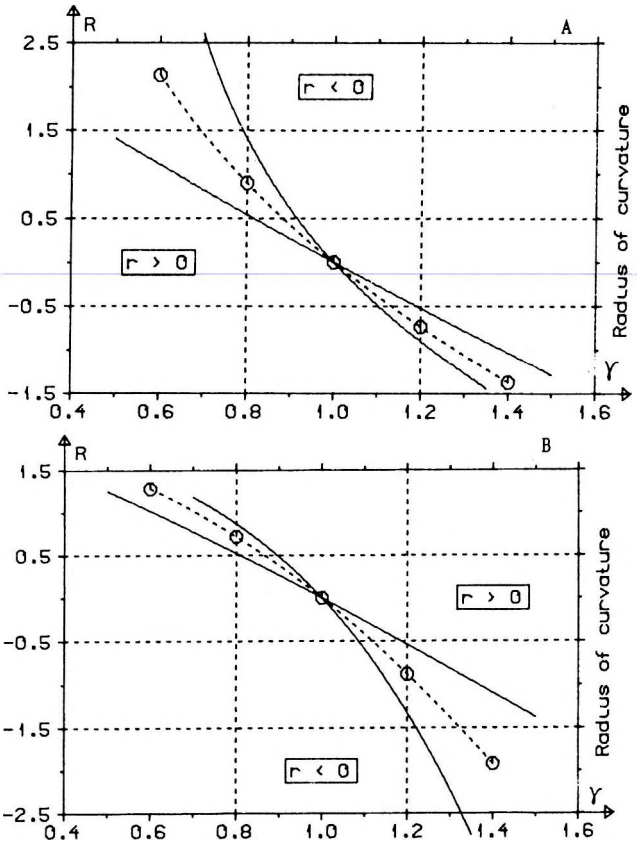


*Fig. 6.* Radius of curvature at the apex of the zero-distance phase front when A—$\eta_* = 2$ km and B—$\eta_C = 2$ km

*6. ábra.* Görbülketi sugár a $t(0)$ fázisfront csúcsán A—$\eta_* = 2$ km és B—$\eta_C = 2$ km esetén

*Рис. 6.* Луч на вершине фазового фронта $t(0)$ А–при $\eta_* = 2$ км В–при $\eta_C = 2$ км

Although Eq. (20) does not apply, in general, to rays making large angles with the $\xi$-axis, it is one of the most important equations in geometrical optics. Hence, if the off-axis position $\xi_C$ has been observed, the lateral position $\xi_D$ of the point diffractor can be recovered from Eq. (20). It must be emphasized that this analysis applies only when symmetry about the $\xi$-axis is present. In general, several foci may appear, so some care must be taken in interpreting the results.

In order to indicate the quality of this analysis, let

$$z = z_0 + A\cos(2\pi x/L)\,, \tag{21}$$

in which case the radius of curvature at $x = 0$ is

$$r = (L/2\pi)^2/A\,. \tag{22}$$

Then, if $A$ = 0.5 km and $L$ = 3 km, it follows that $r \approx 0.5$ km. The rays are displayed in *Figs. 7A* and *7B*, when $\xi_D - \xi_* = 0.0$ km and $\xi_D - \xi_* = 0.5$ km, respectively. Moreover, $\xi_* = 1.5$ km and the velocity ratio $\gamma = 0.75$, in which case it follows that $m \approx 0.5$, $\xi_C - \xi_* \approx 0.25$ km and $\eta_C \approx 1.0$ km. The caustic with the characteristic cusp can easily be identified in each figure. The zero-distance phase front ($f$) is also superimposed on these figures. As a matter of fact, the zero-distance phase front may have cusps and other singular points. The extra time-shift which is needed to obtain the best focus (the position of the cusp) is related to the velocity ratio ($\gamma$) according to Eqs. (17) and (18), respectively. Hence, when $\Delta t$ has been determined by inspection of the migrated output, the velocity ratio can be recovered from the latter equations.

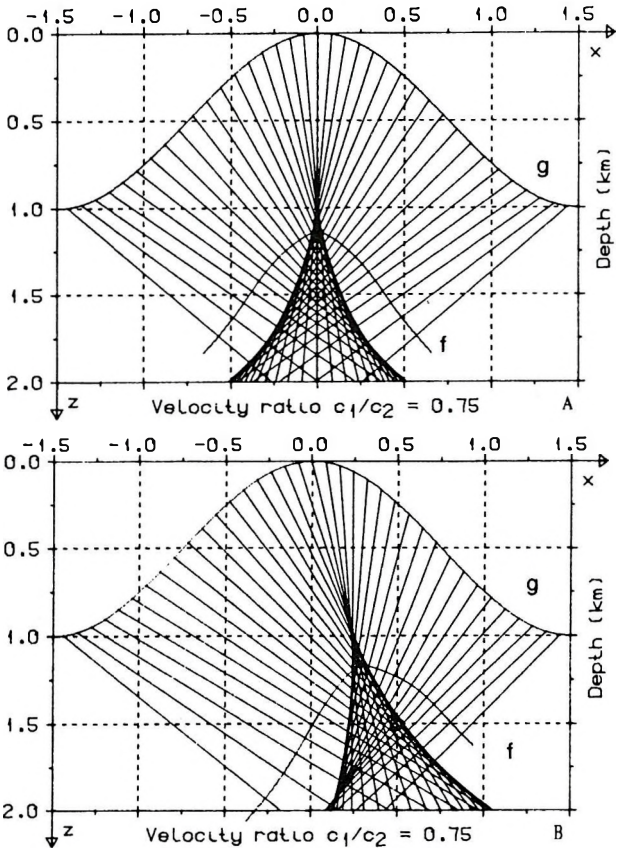


*Fig. 7.* Ray paths when the point diffractor is located A—on the ξ-axis, and B—off the ξ-axis (exp. see Fig. 1)

*7. ábra.* Sugárutak azon esetekben, mikor a diffraktáló pont A—a ξ-tengelyen és B—a ξ-tengelyen kívül helyezkedik el (jelmagyarázat: lásd 1. ábra)

*Рис. 7.* Лучи в случае размещения дифрагирующей точки А–вне оси ξ , В–вне оси ξ . (условные обозначения см. на Рис. 1 )

## 7. Conclusion

A procedure to obtain a velocity macro-model of a 2-D layered medium has been presented. The wave field must be extrapolated from one plane surface to another by wave equation datuming. Conventional migration at the new datum will then properly position the next deeper reflector, but the diffracted energy from a buried point diffractor will be out of focus. As a result, the imaging condition requires artificial adjustments to compensate for the inaccurate treatment of wave propagation. In other words, a compromise that attempts to offset one error by another.

The procedure 'defocuses' diffractions into the zero-distance phase front of refraction. Associated with the zero-distance phase front is the caustic enveloped by the rays. The caustic consists of two branches, and the two branches meet at a cusp. Zero-offset migration with imaging at any time different from zero produces a parallel phase front; hence, the best focus that can be obtained is when a point on a parallel phase front coincides with the position of the cusp. The position of the cusp is determined by the radius of curvature at the apex of the zero-distance phase front.

Interpretation of the migrated sections is part of the process leading to the final velocity. The migration begins at the current datum. No velocity adjustments need to be made below the reflector so migration can be performed with any conventional migration algorithm. The position of the focus and the extra time-shift must be obtained by inspection of the migrated output. On the other hand, once this position and the corresponding time-shift are given, the unknown velocity in the lower layer can be calculated. The wave field is then extrapolated to a new datum by wave equation datuming, and the process continues.

REFERENCES

BERRYHILL J. R. 1979: Wave-equation datuming. Geophysics **44**, 8, pp. 1329-1344

BORN M., WOLF E. 1980: Principles of Optics (6th edition). Pergamon Press

CLAERBOUT J. F. 1971: Toward a unified theory of reflector mapping. Geophysics **36**, 3, pp. 467-481

CORNBLEET S. 1984: Microwave and Optical Ray Geometry. John Wiley & Sons, Ltd.

DOHERTY S. M., CLAERBOUT J. F. 1976: Structure independent velocity estimation. Geophysics **41**, 5, pp. 850-881

FAYE J-P., JEANNOT J-P. 1986: Prestack migration velocities from focusing depth analysis. 56th Ann. Internat. Mtg., Soc. Expl. Geophys., Expanded Abstracts pp. 438-440

GAZDAG J. 1978: Wave equation migration with the phase-shift method. Geophysics **43**, **7**, pp. 1342-1351

MAELAND E. 1989: Focusing aspects of zero-offset migration. Geophysical Transactions **35**, 3, pp. 145-156

YILMAZ O., CHAMBERS R. 1984: Migration velocity analysis by wave-field extrapolation. Geophysics **49**, 10, pp. 1664-1674

## SEBESSÉGBECSLÉS RÉTEGZETT KÖZEGBEN IDŐSZELVÉNY MIGRÁCIÓVAL

Einar MAELAND

Sebesség makromodell becslésére felszín alatti diffraktáló pontokról származó szeizmikus adatok migrációját használja fel, kétdimenziós közegben, dőlő, sík reflektáló felületeket felvéve. A felszíni adatokat új vonatkoztatási szintre extrapolálja az ismert sebességértékekkel, hullámegyenlet módszerrel. Ezután az új felületen állandó sebességű $t_0(x)$ időszelvény migrációt hajt végre. A diffraktált energia ilyenkor nem fókuszálódik, ezért a leképezési feltételt módosítjuk további időtolást figyelembevéve. Ha a diffraktált energia fókuszálódik, a fókusz helyzete és az időtolás mértéke határozza meg a következő rétegben a sebesség értékét. Szintetikus adatokon illusztrálja az analízis minőségi sajátosságait.

## ОЦЕНКА СКОРОСТИ В СЛОИСТОМ РАЗРЕЗЕ С ПОМОЩЬЮ МИГРАЦИИ ВРЕМЕННОГО РАЗРЕЗА

Эинар МЕЙЛАНД

Для оценки скоростной макромодели применяется миграция сейсмических данных от глубинных дифракционных точек. Предполагаются двухмерные плоские наклонные отражающие горизонты. Поверхностные данные при известных значениях скорости методом волнового уравнения пересчитаются на другой уровень, затем выполняется миграция временного разреза $t_0(x)$ при постоянной скорости.

В таком случае дифрагированная энергия не фокусируется, поэтому уточняются условия отображения с учетом смещения времени. Если наблюдается фокусирование дифрагированной энергии, то по положению фокуса и смещению времени определяется скорость для следующего слоя. Особенности анализа иллюстрируются по синтетическим данным.

GEOPHYSICAL TRANSACTIONS 1993
Vol. 38. No. 1. pp. 19-33

# INTEGRATING CHEMICAL AND PHYSICAL LOGGING DATA; EXAMPLES FROM THE OCEAN DRILLING PROGRAM

M. A. LOVELL*, P. K. HARVEY*, R. PELLING* and J. F. BRISTOW*

The successful integration of physical and chemical datasets depends on the nature of the environment under consideration. The datasets may reveal similar features and serve to support the simplest of interpretations, or they may compliment each other in producing different but reconcilable interpretations which would otherwise be unattainable. The Ocean Drilling Program routinely acquires a full suite of physical and chemical logs for most of the holes drilled. In Hole 762 on the Exmouth Plateau the physical and chemical data identify different features of a sedimentary environment; the physical characteristics relate to the major changes in lithology whilst the chemical resolve the thin clay beds within the sequence. In Hole 504B in the Eastern Equatorial Pacific similar relationships are visible in crystalline basement. The physical logs respond to a general decrease in porosity with depth, whilst the chemical logs reflect the different modes of alteration which have contributed to the evolution of this young section of ocean floor. In the Indian Ocean, Hole 735B sampled tectonically emplaced gabbros with excellent core recovery. The physical and chemical data both identify the lithological variations with the chemical data enabling the identification of individual lithologies. Conversion of the chemical data to a meaningful mineralogical assemblage is attempted as a suggested route to constraining physical properties. The difficulties in apportioning the chemistry to the mineralogical assemblage are numerous but integration of the chemical and physical data can assist in certain situations. Data from Hole 799B are used to illustrate the use of density measurements to constrain the proportions of two minerals with compositional colinearity (quartz and opal).

**Keywords: geochemical well logging, oceanic crust, porosity, resistivity**

* Borehole Research, Department of Geology, University of Leicester, Leicester, LE1 7RH, UK.

Manuscript received: 14 October, 1991

## 1. Introduction

The geological interpretation of wireline logs relies traditionally on the evaluation of a series of physical and limited chemical responses which are observed in the field of electrical, acoustic, and nuclear measurements. Considerable success has been achieved in calibrating such response, predominantly in an empirical manner, in both sedimentary and crystalline successions. The recent advances in nuclear techniques have expanded the range of quantifiable measurements into the field of geochemistry [ANDERSON et al. 1990, HARVEY, LOVELL 1989, LOVELL, ANDERSON 1989] such that it is now feasible to determine in situ quantitative data relating to the majority of the major elements present in most common rock types. The advent of quantitative geochemical logging provides the interpreter with a means of assessing a different facet of a rock, and in turn opens up the possibility of identifying the relative proportions of individual components.

The Ocean Drilling Program routinely acquires a full suite of conventional wireline logs, including FMS images [see Ocean Drilling Program Wireline Logging Manual 1989]. In addition, using a combination of nuclear tools the following parameters are typically determined:

K Th U Fe Si Al Ca S H Ci Ti Gd Al bulk density / photo electric factor (PEF).

The elemental suite comprises all major elements anticipated to be present within the Oceanic Crust with the exception of Na and Mg. Na is dominated by the presence of sea-water. It is, however, possible to determine an estimate of the amount of (Na and Mg) for the PEF measurement by recomputing the PEF from the elemental concentrations and assuming the residual PEF is attributable to these two elements. Whilst the errors involved in such a manipulation can be considerable there may be specific situations where a relative magnitude, particularly for Mg, is valuable.

This paper concentrates on the integration of chemical concentrations with conventional logging data in scientific investigations of the oceanic crust. The results presented here pertain to a variety of geological environments within the world's oceans and are the product of the efforts by numerous scientists who have participated in the Ocean Drilling Program. It is only possible within the remit of this paper to consider a few select examples of the integration of physical and chemical logs.

## 2. Chemical and physical integration

The traditional wireline logging measurements such as sonic velocity, electrical resistivity, density and total natural gamma ray may be classified as physical logs in comparison with the more recent developments in spectral chemical logs. This division is in some ways unfortunate since it is only through

the integration of the data that we can hope to advance our scientific understanding of the complex Earth.

### *Hole 762, Exmouth Plateau*

A comparison of the two datasets can, however, show their complimentary and hence mutually supportive nature. Hole 762 was drilled on the Exmouth Plateau in a sedimentary section. The results [Shipboard Scientific Party 1989b] are plotted in *Fig. 1* and show the dramatic changes in depositional environment as exhibited by a range of logs. The sequence passes from silts and clays of the Barrow delta up through a transgressive siltstone sequence to pelagic nannofossil chalks. These are identified clearly by the physical logs but the chemistry only appears to pick out the high Si zone of the transgressive sequence. Higher up the sequence the variations in the Si, Ca and Al curves identify high frequency fluctuations in clay content within the chalk. These variations, which are probably climate related, are not recorded by the physical logs because of the small changes in physical parameters which they produce.

### *Hole 504B, Costa Rica Rift*

The definition of primary lithology allows the formation to be allocated to a position within an overall framework of rock descriptions. Superimposed on this basic characterisation which pertains to its mode of formation, however, may be effects of subsequent processes involving variations in temperature or pressure, or perhaps fluids of varying compositions flowing through the rock. These processes may be sufficient to completely change the character of the rock, and hence its lithology, or they may have less substantial but measurable effects on the formation.

Hole 504B in the Eastern Equatorial Pacific is perhaps the most famous attempt by any drilling initiative to drill deep into the ocean crust. As such it is the only hole in the ocean crust to sample both the overlying sediments, pillow basalts and basalt dikes which are analogous respectively to Layers 1, 2A and 2B of the classic ocean floor layer cake defined by seismologists [KIDD 1977]. The history, success and failure of attempts at the hole over the last decade are well documented by BECKER et al. [1989]. The hole is located on the southern flanks of the Costa Rica Rift, a mid-ocean volcanic spreading ridge, in 5.9 million year's old crust. As such it penetrates over 1300 metres of basaltic rock. The lithology of this basement section is notably uniform throughout and is separated into three separate zones, primarily on the basis of its physical attributes, particularly with respect to its supposed mode of emplacement. Thus the upper zone is dominated by pillows, the lower zone by dikes, with a substantial transition between, extending from approximately 845 mbsf to

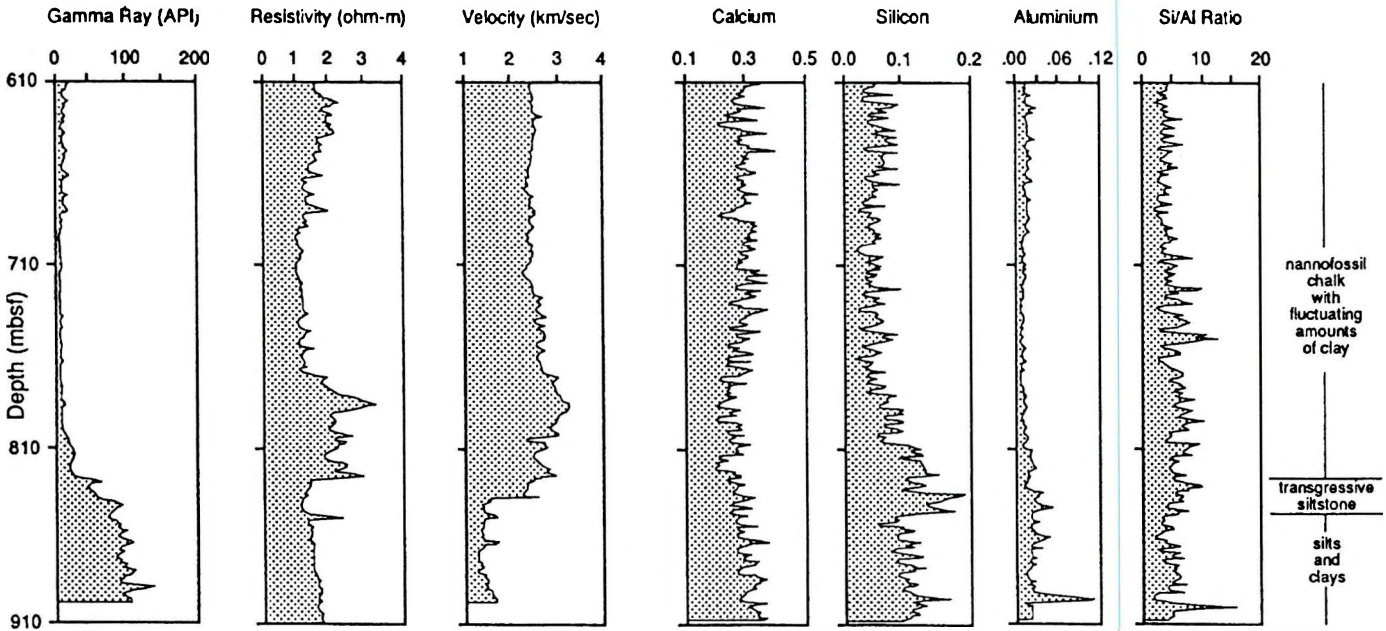


*Fig. 1.* Geophysical and geochemical logs contrasted for ODP Hole 762 on the Exmouth Plateau. Note the geophysical logs primarily respond to major changes in lithology while the geochemical logs resolve the thin clay beds occurring higher up within the chalk

*1. ábra.* Az Exmouth Plató 762 jelű fúrására vonatkozó geofizikai és geokémiai lyukszelvények összehasonlítása. Figyeljük meg, hogy a geofizikai lyukszelvények elsősorban a nagy litológiai változásokat jelzik, míg a geokémiai szelvények a krétában magasabban előforduló vékony agyagrétegeket is feltárják

*Рис. 1.* Сопоставление геофизических и геохимических данных по скважине Эксмут плато 762. По геофизическим данным прежде всего выявляются крупные литологические изменения, а по геохимическим данным также обнаруживаются и тонкие прослойки глины в меле

1055 mbsf. Examination of the conventional logging suite identifies these trends as a result of the decrease in porosity with depth (*Fig. 2*), from porous rubbly zones at shallow depth (an aquifer occurs near the top of the basement section) to a very dense, low porosity zone at the base of the hole [Shipboard Scientific Party 1988a].

In comparison, however, the continuous geochemistry derived from the downhole nuclear measurements exhibits two separate features. Firstly, the overall trends can be identified as in the core and conventional logs. But in addition fine scale variations may be identified within each major zone [HARVEY, LOVELL 1989]. The overall alteration boundaries of ALT et al. [1985] are also identified by the nuclear measurements (*Fig. 3*).

Integration of these two interpretations enables both the primary emplacement and secondary alteration effects to be observed within this one hole.

### *Hole 735B, Atlantis II Fracture Zone*

Ocean Drilling Program Site 735 is located on a shallow platform on the east rim of the Atlantis II Fracture Zone in the SW Indian Ocean where a series of gabbroic rocks have been tectonically emplaced at the surface. Hole 735B penetrates to a depth of 500.7 mbsf and is well characterised by the core descriptions on account of its 87% recovery. The petrographic descriptions clearly identify a range of different lithologies within the hole [Shipboard Scientific Party 1989a]. *Figure 4* shows this lithostratigraphy together with a selection of the in situ physical and chemical data. Both datasets identify the major stratigraphic boundaries, particularly the iron-titanium rich gabbro layer in the middle of the section, bounded on either side by comparatively iron-titanium poor gabbros. Using the nuclear derived elemental data from downhole measurements, PELLING et al. (in press) have used a statistical technique to define groups of similar chemical character down the hole. Their results show both the excellent quality of the downhole nuclear data and the power of the Iterative Non-hierarchical Cluster Analyses (INCA) technique to define changes in lithology from the log data.

## 3. Mineralogical estimation

The end product of both the lithology and alteration studies are inextricably related. Since they rely on the same data it is inevitable that often the analysis will be complicated by attempting to find two different routes, both of which are separate facets of one complex rock. An alternative approach to the mathematical or statistical manipulation of the geochemical data is to produce a unique transformation of the elemental data into a mineralogy log. The interpretation of this derived-mineralogy then enables the study of the

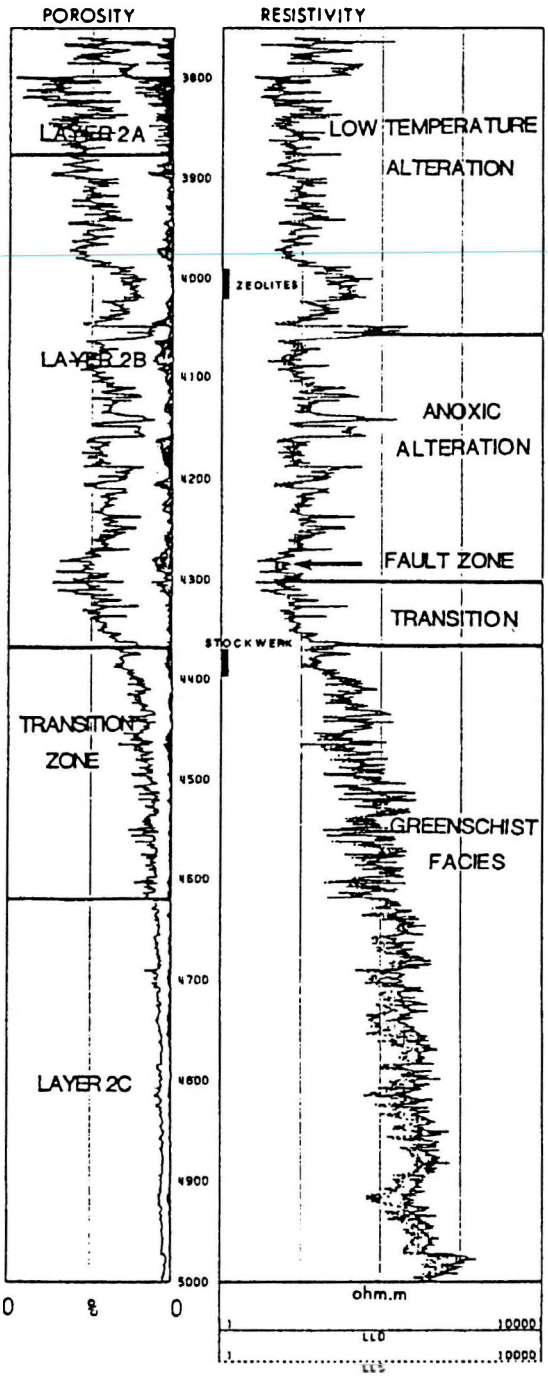


*Fig. 2.* Electrical resistivity and derived-porosity for Hole 504B showing the decrease in pore space and the consequent increase in resistivity with depth [after PEZARD, ANDERSON 1989]

*2. ábra.* Az 504B fúrásra vonatkozó elektromos ellenállás és porozitás görbék a mélységgel csökkenő pórustérfogatot és ennek megfelelően a mélységgel növekvő ellenállást mutatják [PEZARD, ANDERSON 1989 nyomán]

*Рис. 2.* По скважине 504B кривые электрического сопротивления и пористости показывают уменьшение с глубиной объема пор и, соответственно, увеличение с глубиной сопротивления [по PEZARD, ANDERSON 1989]

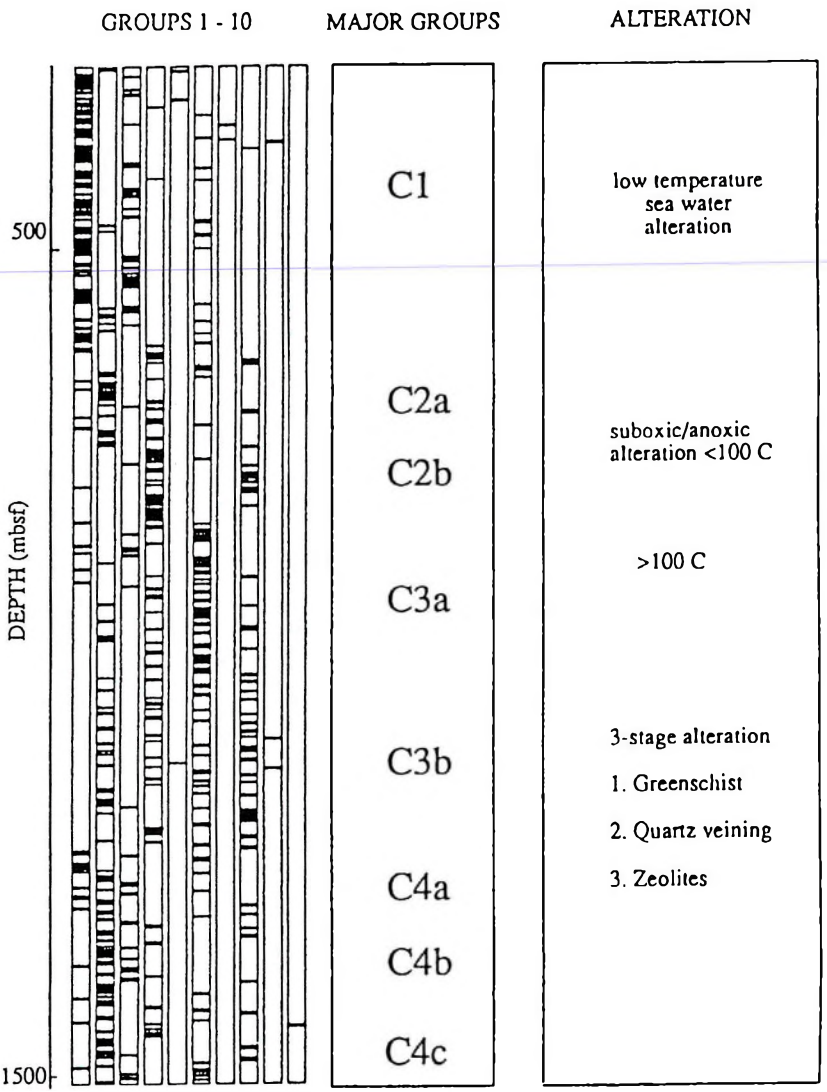


*Fig. 3.* Major geochemical groups derived from a statistical classification compared with core based alteration studies of Hole 504B in the Eastern Equatorial Pacific [after LOVELL et al. 1990]

*3. ábra.* A Kelet-Ekvatoriális Pacifikum 504B jelű fúrására elvégzett statisztikus osztályozásból számított fő geokémiai csoportok és a magmintákon alapuló vizsgálatok összehasonlítása [LOVELL et al. 1990 nyomán]

*Рис. 3.* Сопоставление данных анализа кэрна и главных геохимических групп, расчитанных по статистической классификации по скважине Восточно-экваториальный Тихий океан 504B [по LOVELL et al. 1990]

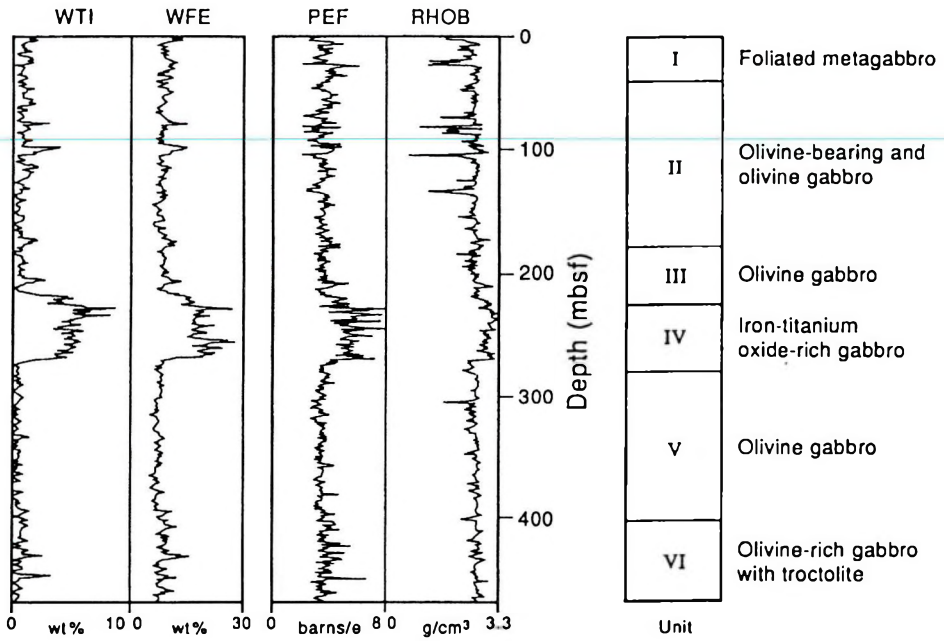


*Fig. 4.* Lithostratigraphy of Hole 735B in the Indian Ocean. The physical and chemical downhole logs both identify the major distinctions. Note in particular the high iron-titanium gabbro in the middle of the section separated by the uniform gabbros below by a low denity (high porosity) fracture zone. WTI and WFE are GLT derived weight percent of iron and titanium respectively, PEF is photoelectric factor, RHOB is density

*4. ábra.*. Az Indiai Óceán 735B fúrásának litosztratigráfiája. Mind a fizikai, mind a kémiai lyukszelvények alapján azonosíthatók a fő változások. Különösen figyelemreméltó a szelvény közepén látható magas vas-titán tartalmú gabbró, amelyet az alatta található egységes gabbróktól egy kis sűrűségű (nagy porozitású) töréses zóna választ el. A WTI és a WFE a GLT-vel számított vas illetve titán tömegszázalék, a PEF fotoelektromos tényező, a RHOB pedig sűrűség

*Рис. 4.* Литостратиграфия скважины Индийский океан 735в. Основные изменения выявляются как и по физическим, так и по химическим данным. Отмечается, что выявленное в середине разреза габбро с высоким содержанием железа и титана отделяется от выявленных ниже габбро разломной зоной высокой пористости. WFE, WTI весовое содержание железа и титана, рассчитанные по GLT, PEF фотоэлектрический коеффициент, RHOB плотность

variations in both lithology and alteration downhole. An attempt at calculating the downhole mineral assemblages in Hole 504B is documented in ANDERSON et al. [1990].

The transformation of elements into minerals is a process which has been used for considerable time by geologists [BARTH 1959, MIESCH 1962]. The inversion is, however, at least as difficult as any other inversion problem, but is complicated by the extensive range of mineral possibilities, both in terms of individual types present, and their compositional ranges. HARVEY et al. [1990] provide a recent substantial review of the problem and suggest a number of alternative solutions as well as identifying some major areas of difficulty. Ideally, knowledge of the minerals present together with their composition is essential for a well constrained solution. Unfortunately, such a situation is rarely observed.

*Figure 5* shows the results of a mineralogical transformation using the downhole geochemistry from Hole 735B in the Indian Ocean (compare with Fig. 4). Although further detailed core mineralogy is awaited the overall mineralogy appears to fit reasonable well with visual descriptions. In particular the Fe-Ti oxide rich layer of Unit IV is clearly defined and is seen to overlie the relatively uniform, olivine poor, gabbro of Unit V. The model in Fig. 5 was generated using a euclidian distance algorithm [see HARVEY, LOVELL 1991 for details of this technique] in which the mineral assemblage was chosen at each depth interval from a selection of twelve possible assemblages. These assemblages all contained plagioclase, clinopyroxene, magnetite, ilmenite and pyrite as essential phases, but differed in the composition of the plagioclase and clinopyroxene, and the presence or absence of orthopyroxene and olivine. Model plagioclase compositions varied from An61 to An74 and it is encouraging that the most commonly selected mineral assemblage (plagioclase-clinopyroxene-orthopyroxene-magnetite-limenite-pyrite) contains a plagioclase of An61, very close to the petrographically determined median value. The opaque phases were modelled using magnetite and ilmenite as individual minerals, there being no information at present about the degree of solid solution present between the minerals. The precise nature of the opaque phases is of particular interest in further resolving this section. The standard error log (SErr) in Fig. 5 shows overall good agreement between the fitted mineralogy log and input chemistry, the average error over the whole log being 0.46%.

HARVEY, LOVELL [1991] discuss the difficulties faced in assigning elements to minerals when there are several phases present which are compositionally the same. This problem typically causes difficulties in sedimentary environments where there is a varying input of terrigenous quartz and biogenic opal. Both are chemically the same ($SiO_2$) but are mineralogically and sedimentologically very different. Indeed the interpretation of the environment of deposition relies on the identification of the proportions of each present. One approach to this problem is to utilise the density log as an indicator of the proportions of each component present [BRISTOW 1991]. *Figure 6* shows the result of this approach from well 799B drilled on Ocean Drilling Program Leg 128. The hole is situated in the Kita Yamato Trough, a failed backarc rift

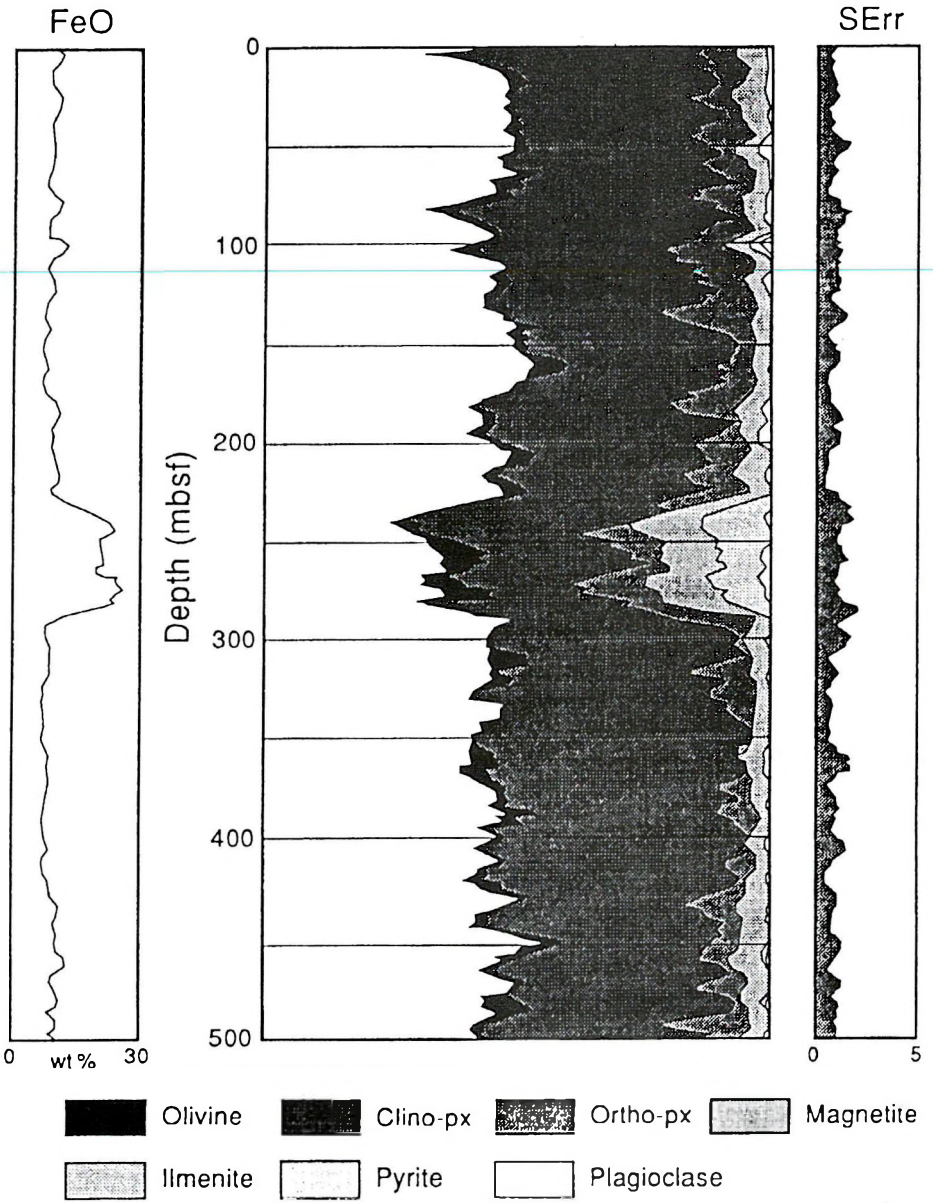


*Fig. 5.* Mineralogical transformation of the downhole geochemistry data for Hole 735B. Note the lithostratigraphy and logs showh in Fig. 4. SErr is standard error

*5. ábra.* A 735B fúrólyukban mért geokémiai adatokból számolt ásványos összetétel. Figyeljük meg a 4. ábrán látható litosztratigráfiát és a lyukszelvényeket. Az SErr a standard hibát jelöli

*Рис. 5.* Минеральный состав, определенный по геохимическим данным по скважине 735B. Литостратиграфия и разрезы скважины изображены на Рис. 4. SErr—стандартное отклонение

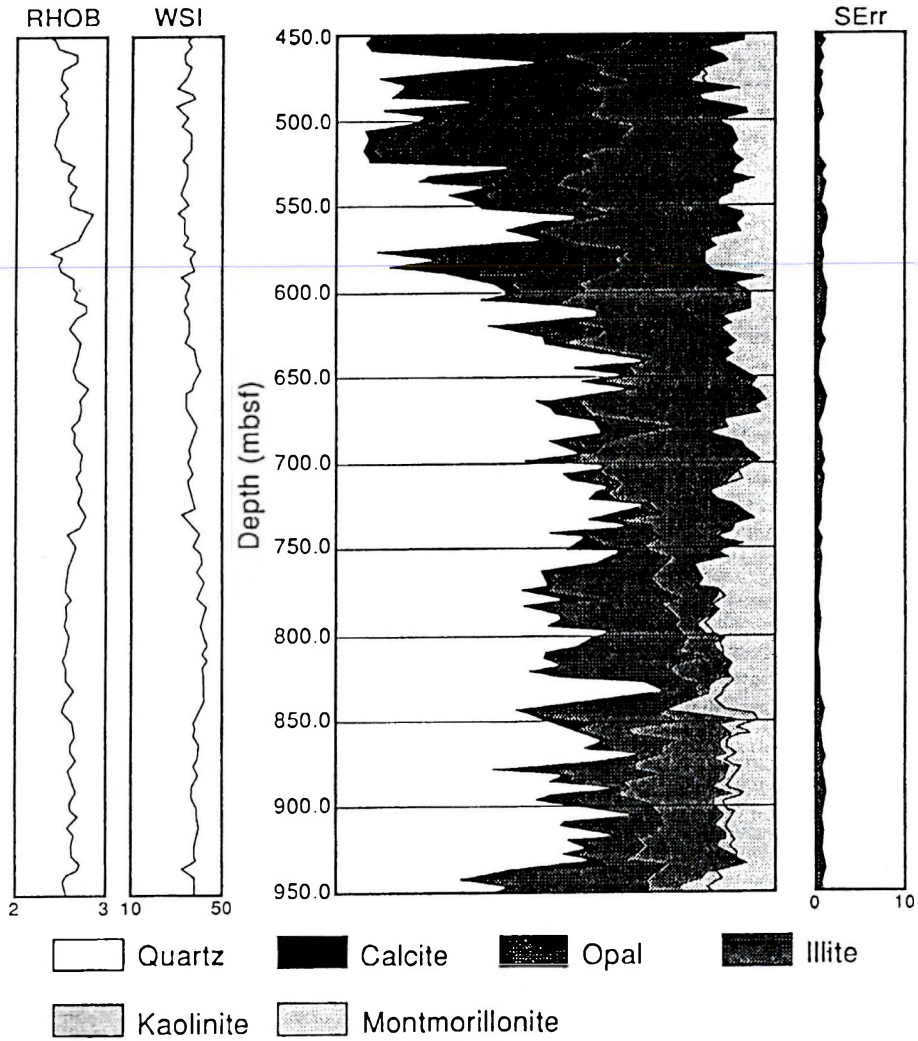


*Fig. 6.* Mineralogical transformation of the downhole geochemistry data from Hole 799B in the Kita Yamato Trough. SErr is standard error, RHOB is density, and WSI is weight percent of silicon

*6. ábra.* A Kita Yamato-árok 799B fúrólyukában mért geokémiai adatokból számolt ásványos összetétel. Az SErr a standard hibát, az RHOB a sűrűséget, a WSI pedig a szilikon tömegszázalékot jelöli

*Рис. 6.* Минеральный состав, определенный по геохимическим данным скважины Малая Ямато впадина 799B. SErr—стандартное отклонение; RHOB—плотность; WSI—весовое содержание кремни

environment in the Sea Japan. This Miocene sequence of sediments shows the palaeoceanographic evolution of the Sea of Japan. A palaeoclimate record of the region is recorded in the periodic changes in the abundance of biosiliceous and biocalcareous material and the terrestrially derived aeolian dust. The mineralogy log shown in figure 6 is determined by an inversion of the downhole GLT derived geochemistry using a geometric method. Although compositionally colinear, quartz and opal-CT have different matrix densities. They are differentiated in the model by using an input matrix density curve, calculated from the density tool. The results agree with the qualitative core descriptions and indicate in more detail the variation of quartz and opal with depth throughout the hole.

## 4. Discussion

The use of nuclear logs has heralded the opening up of the field of log-interpretation to geochemists and mineralogists, together with geologists involved in studying structure, pore fluids, and processes. The in situ chemical signatures provide detailed observations of the variations in but one more facet of the complex character of a rock. This observation is effectively continuous downhole and at in situ conditions.

In order to utilise fully the downhole data it is important that the strictest control is observed during data acquisition and processing. Calibration of the datasets and evaluation of error both in raw data and derived parameters must form the basis of further studies if the potential embedded in the integration of data is to be realised.

Combining this excellent and in many ways novel data with conventional log data and core data represents a major task. The provision of meaningful quantitative mineralogical assemblages should yield better constraints on the physical properties of the formation and enable a global geological character to be established on a continuous basis throughout the borehole.

## Acknowledgements

The innovative downhole measurement program within the Ocean Drilling Program and the interpretation of the huge database represents a massive collaborative venture on the part of both industry and academia in a truly international context. This paper is one of the many results of that success, and we acknowledge the help of all those who have contributed to both the success of the Ocean Drilling Program downhole measurements initiative and to individual log interpretations. Particular thanks go to Roger ANDERSON and the staff of the Borehole Research Group at LDGO, Columbia University. This

work has been supported in various ways by the Natural Environment Research Council.

## REFERENCES

ALT J. C., LAVERNE C., MUEHLENBACHS K. 1985: Alteration of the upper oceanic crust: mineralogy and processes in Deep Sea Drilling Project Hole 504B, Leg 83. *In:* Anderson, R. N., Honnorez, J., Becker, K. et al.: Initial Reports of the Deep Sea Drilling Program, **83**, US Government Printing Office, Washington, pp. 217-224

ANDERSON R. N., ALT J. C., MALPAS J., LOVELL M. A., HARVEY P. K., PRATSON E. L. 1990: Geochemical well logging in basalts; the Palisades Diabase Sill and the Oceanic Crust of Hole 504B, Eastern Equatorial Pacific. J. Geophy. Res. **95**, pp. 9265-9292

BARTH T. F. W. 1959: Principles of classification and norm calculation of metamorphic rocks. Journal of Geology **67**, pp. 135-152

BECKER K. et al. 1989: Drilling deep into the oceanic crust, Hole 504B, Costa Rica Rift. Rev. Geophys. **27**, pp. 79-102

BRISTOW J. F. 1991: Preliminary interpretation of downhole logs from Ocean Drilling Program Leg 128. Report BR91/JFBO1. University of Leicester (Department of Geology) Leicester, UK

HARVEY P. K., LOVELL M. A. 1989: Basaltic Lithostratigraphy of Deep Sea Drilling Program/Ocean Drilling Program Hole 504B. Nuclear Geophysics **3**, pp. 87-96

HARVEY P. K., BRISTOW J. F., LOVELL M. A. 1990: Mineral transforms and downhole geochemical measurements. Scientific Drilling 1, pp. 163-176

HARVEY P. K., LOVELL M. A. 1991: Downhole mineralogy logs: the problem of compositional colinearity in mineral inversion. *In*: Hurst A, Worthington P, Griffiths C. (eds.) Geological Applications of Wireline Logs Rides Again!

KIDD R. 1977: A model for the process of formation of the upper oceanic crust. Geophys. J. Royal Astron. Soc. **50**, pp. 149-183

LOVELL M. A., ANDERSON R. N. 1989: When downhole logging turns to geochemistry. Geology Today, September-October, pp. 164-166

LOVELL M. A., HARVEY P. K., ANDERSON R. N. 1990: The application of Nuclear Logs in the Ocean Drilling Program. IEEE Trans. on Nucl. Sci. **37**, pp. 1366-1393

MIESCH A. T. 1962: Computing mineral composition of sedimentary rocks from chemical analysis. J. Sediment. Petrol. **32**, pp. 217-225

Ocean Drilling Program Wireline Logging Manual 1989. Volume 2, 2nd. edition. LDGO, (Palisades 10964 New York)

PELLING R., HARVEY P. K., LOVELL M. A., GOLDBERG D. 1991: Statistical analysis of geochemical logging tool data from Ocean Drilling Program Hole 735B, Atlantis II fracture zone, SW Indian Ocean. Proceedings. Ocean Drilling Program, Scientific Results 118. College Station, TX. (in press)

PEZARD P. A, ANDERSON R. N. 1989: Morphology and alteration of the upper oceanic crust from in situ electrical experiments in Deep Sea Drilling Project Hole 504B. *In*: Becker K. Sakai, H. Merill R. et al.: Proceedings Ocean Drilling Program, Scientific Results, **111**, 97-108, Ocean Drilling Program, College Station, Texas

Shipboard Scientific Party, 1988a: Proceedings. Ocean Drilling Program 111, Volume A, College Station, TX

Shipboard Scientific Party, 1989a: Proceedings. Ocean Drilling Program 118, Volume A, College Station, TX.

Shipboard Scientific Party, 1989b: Proceedings. Ocean Drilling Program 122, Volume A, College Station, TX.

## A KÉMIAI ÉS FIZIKAI KAROTÁZS ADATOK INTEGRÁLÁSA; PÉLDÁK AZ ÓCEÁNI MÉLYFÚRÁSI PROGRAMBÓL

M. A. LOVELL, P. K. HARVEY, R. PELLING és J. F. BRISTOW

A fizikai és kémiai adathalmazok sikeres integrálása a vizsgált környezet természetétől függ. Az adathalmazok feltárhatnak hasonló jellegzetességeket és segíthetnek megerősíteni a legegyszerűbb értelmezést, vagy kiegészíthetik egymást, ha olyan különböző, de összeegyeztethető értelmezést adnak, mely más módon nem lenne hozzáférhető. Az Óceáni Mélyfúrási program a legtöbb fúrásra fizikai és kémiai karotázs-szelvények egész sorát alkalmazza rutinszerűen. Az Exmouth Plató 762-es számú fúrásánál a fizikai és kémiai adatok az üledékes környezet különböző vonásait azonosítják; a fizikai jellemzők a litológia fő változásaira vonatkoznak, míg a kémiaiak feltárják a sorozaton belüli vékony agyagrétegeket. A Kelet-Ekvatoriális Pacifikum 504B jelű fúrásában hasonló összefüggések láthatók a kristályos aljzatban. A fizikai lyukszelvények a mélységgel csökkenő porozitásra érzékenyek, míg a kémiai lyukszelvények ennek a fiatal óceánmedernek a fejlődését elősegítő különböző változásokat tükrözik. Az Indiai-óceánban a 735B jelű fúrás tektonikailag áthelyezett gabbróból vett mintát kitűnő magkihozatallal. Mind a fizikai, mind a kémiai adatok azonosítják a litológiai változásokat, a kémiai adatok pedig lehetővé teszik az egyedi litológiai jellemzők azonosítását. A kémiai adatokból megpróbáltuk meghatározni az adott ásványtani együttest és így azt reméltük, hogy a lehetséges fizikai tulajdonságokat is le tudjuk szűkíteni. A kémiai adatokból az ásványtani együtteseket igen nehéz meghatározni, de a fizikai és kémiai adatok integrálása bizonyos helyzetekben segíthet. A 799B fúrásból származó adatokat használjuk annak illusztrálására, hogy a sűrűségmérések segítségével hogyan lehet két, azonos összetételű ásvány (kvarc és opál) arányát meghatározni.

## ИНТЕГРАЦИЯ ДАННЫХ ХИМИЧЕСКОГО И ФИЗИЧЕСКОГО КАРОТАЖА, ПРИМЕРЫ СКВАЖИН НА ОКЕАНЕ

М. А. ЛОВЕЛЛ, П. К. ХЕРВЕЙ, Р. ПЕЛЛИНГ и Дж. Ф. БРИСТОУ

Удачность интеграции физических и химических данных зависит от природы изучаемой среды. Они могут выявить сходные особенности, тем самым, подтвердить простейшую интерпретацию данных, или привести к разной но сопоставимой интерпретации и, тем самым, дополнять друг друга. В программе бурения скважин на океанах предусматривается проведение целого ряда видов химического и физического каротажа. По скважине Эксмут плато 762 по физическим и химическим данным определяется характеристика осадочных образований: физические параметры показывают основные изменения литологического состава, а по химическим данным выявляются глинистые прослойки внутри комплексов.

По скважине Восточно-экваториальный Тихий Океан 504B показывается характеристика кристаллического фундамента. Физические параметры чувствительны к

уменьшению с глубиной пористости, а по химическим данным прослеживаются изменения, способствующие развитию молодого океана. На Индийском океане из скважины 735B получен образец тектонически перемещенного габбро при отличном выходе кэрна. Как и по химическим, так и по физическим данным выделяются изменения литологического состава образований, а по химическим данным можно выявить их литологические особенности.

Была выполнена попытка определить парагенетическую ассоциацию минералов по химическим данным и, таким образом, ограничивать возможные их физические параметры. По химическим данным затруднено определение парагенетической ассоциации минералов, но интеграция химических и физических данных в некоторых случаях может помогать в решении задачи. По данным скважины 799B показывается пример определения соотношения содержания двух сходных по составу минералов (кварц и опал) по данным измерений плотности.

GEOPHYSICAL TRANSACTIONS 1993
Vol. 38. No. 1. pp. 35-46

# RELATIONSHIP OF POROSITY AND PERMEABILITY TO MERCURY INJECTION DERIVED PARAMETERS FOR SANDSTONES OF THE TÖRTEL FORMATION, HUNGARY

Abdel Moktader A. EL-SAYED*

Mercury injection-capillary pressure tests are expensive and, therefore, are not extensively used. However various petrophysical parameters derived from them are valuable with regard to both reservoir geology and engineering. Pore aperture size estimated from mercury injection tests has been used to evaluate seals for stratigraphic hydrocarbon bearing traps. Mercury injection-capillary pressure curves of 45 sandstone core samples obtained from the Törtel Formation (Algyő oil and gas field) were investigated.

This paper develops empirical equations for estimating pore aperture size and some important reservoir parameters from routine core analysis (porosity and/or permeability). Pore aperture sizes $r_{36}$ and $r_{50}$ were estimated. Size $r_{50}$ seems to be critical and the most effective pore size for delineating hydrocarbon traps in the Törtel Formation. In addition, the mercury recovery efficiency could be estimated.

**Keywords: capillary pressure, porosity, permeability, Törtel Formation, Hungary**

## 1. Introduction

The Törtel Formation (Pannonian s.l.) is mainly composed of bedded sandstones intercalated with siltstones, marls, lignites and carbonified plant fragments. Sandstone bodies were interpreted as distributary channel, barrier and mouth bars, and deltaic fringe deposits [EL-SAYED 1981, BÁN, EL-SAYED 1987, JUHÁSZ 1991]. Limonitic concretions are common in the stratified laminated and cross-laminated medium of fine grained sandstones and siltstones. The environment of deposition of the Törtel Formation varies from

* Ain Shams University, Dept. of Geology, Cairo, Egypt

Manuscript received: 27 May, 1992

shallow lake and fluvial marsh to terrestrial and fluvially dominated delta [MUCSI, RÉVÉSZ 1975, EL-SAYED 1981, BÉRCZI, PHILLIPS 1985].

The Törtel Formation in the Great Hungarian Plane is underlain by the Algyő Formation and overlain by the Zagyva Formation. In the Algyő field it is penetrated by more than 900 drilled holes. Five superimposed hydrocarbon bearing reservoirs were attributed to the Törtel Formation. They are, from bottom to top: Algyő-1, Algyő-2, Szeged-1, Szeged-2 and Szeged-3. The Algyő-2 reservoir sequence was petrophysically studied by EL-SAYED [1981 and 1983], and classified into three deltaic rock genetic types. The previously mentioned reserviors are considered as the most important oil producing sequences in the Algyő field. The reservoir characteristics of them are available in the literature [EL-SAYED 1991, EL-SAYED, VOLL 1992].

Petrophysicists are interested in how porosity and permeability relate to pore throat size distribution especially in reservoir rocks. However, exploration geologists are interested rather in using pore aperture size derived from mercury injection-capillary pressure tests to evaluate the sealing capacity of cap rocks [BERG 1975, MAGARA 1978]. Hydrocarbon migration problems have been discussed by number of authors [e.g. SOMFAI 1976, WARDLAW, CASSAN 1979, SCHOWALTER 1979, SWANSON 1981]. Hydrocarbon migration and entrapment result from the interaction between buoyant pressures and capillary forces.

In reservoir rocks, the minimum pressure necessary to force the oil (usually the non-wetting phase) to enter the rock pores is known as displacement pressure [SCHOWALTER 1979]. It is defined as the pressure at 10 % mercury saturation on the mercury injection-capillary pressure curve. However, the pore aperture size corresponding to it can be determined. It is used for both reservoir and sealing capacity evaluation. Therefore a readily available estimation of displacement pressure from routine core analysis would be helpful.

Another parameter of interest is the pore aperture size that corresponds to the apex of a hyperbola on the mercury injection-capillary pressure plot [THOMEER 1960]. This parameter has the potential for depicting stratigraphic oil bearing traps [SWANSON 1977, PITTMAN 1989 and 1992]. PITTMAN [1992] showed that the net thickness of sandstone reservoirs having the 36th percentile of mercury saturation, which corresponds to a pore aperture size greater than 0.5 μm (5000 Å), was useful for delineating the charged stratigraphic traps. He introduced useful empirical equations for estimating various reservoir parameters especially for sandstones.

The pore/throat size ratio is a parameter thought to be related to the microscopic recovery efficiency of the non-wetting phase in sandstone reservoirs [WARDLAW 1980, KOPASKA-MERKEL, FRIEDMAN 1989, MORAES 1991]. The oil recovery efficiency decreases while the pore/throat size ratio increases. On the other hand, the opposite regime is obtained for the recovery efficiency of the rock-saturating wetting phase. The purposes of this study are (1) to detect which percentile of cumulative mercury saturation is able to give reliable results in trap delineation for the sandstones of the Törtel Formation,

(2) to present empirical relationships between porosity ($\Phi$), permeability ($k$) and capillary pressure derived parameters.

## 2. Methodology

Forty five porosity and nitrogen permeability analyses were available in Hungarian Hydrocarbon Institute (SZKFI) files on plugs that had also been used for mercury injection tests of sandstone samples obtained from the Törtel Formation. The porosities and permeabilities of the data set ranged from 8.1 % to 30 % and from 0.03 md to 3000 md respectively. The studied samples were mainly of calcareous and argillaceous sandstones and siltstones.

The displacement pressure is determined graphically from the mercury injection curves, whereas the corresponding pore aperture radii were calculated by using the equation adapted from WASHBURN [1921]:

$$P_c = -2\,\gamma\cos\Theta/r \tag{1}$$

where $P_c$ is capillary pressure (dynes/cm$^2$), $\gamma$ is the surface tension of mercury (480 dynes/cm), $\Theta$ is the contact angle of mercury in air (140 °C) and $r$ is the radius of pore aperture for a cylindrical pore. Thus, $r$ (μm) = $107/P_c$ (psia).

The mercury recovery efficiency ($Re$) is calculated in accordance with the equation introduced by HUTCHEON and OLDERSHAW [1985]:

$$Re = (S - S_r)/S \tag{2}$$

where $S$ is the volume of mercury injected at maximum pressure (cc) and $S_r$ is the volume of mercury retained in the pore system at minimum pressure (cc). Both $S$ and $S_r$ are measured on capillary curves. However, the microscopic oil recovery efficiency ($Re_o$) was calculated by MORAES [1991] for oil-saturated samples as:

$$Re_o = (So_{\max} - Sor_{\min})/So_{\max} \tag{3}$$

where $So_{\max}$ is the maximum oil saturation and $Sor_{min}$ is the minimum residual oil saturation.

The apex of the curves of *Fig. 1A* was calculated graphically by using SWANSON's method [1977]. He determined that the 45° line is tangential to the hyperbola of a log-log plot at the apex. Consequently, the average apex of the sandstone samples of the Törtel Formation is calculated by plotting the mercury saturation at the defined apex divided by the mercury saturation pressure on the $y$ axis against the mercury saturation on the $x$ axis for each mercury injection curve (*Fig. 1B*). A regression analysis program [STOQDLEY 1984] was used to establish various empirical relationships.

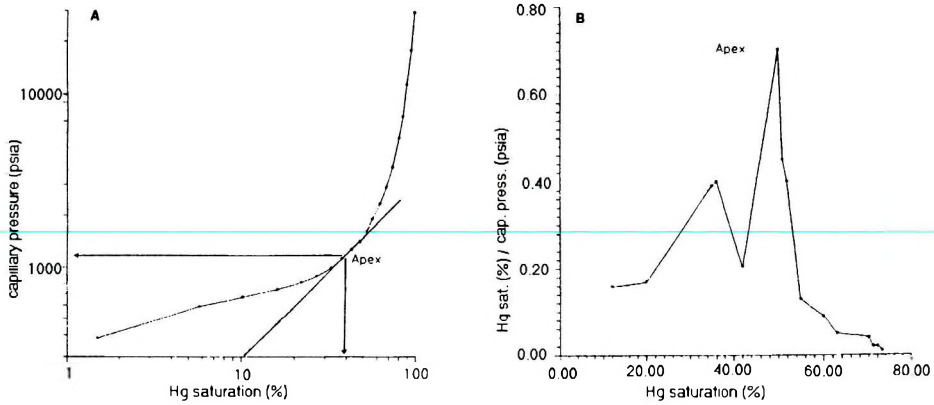


*Fig. 1.* A—Log-log hyperbolic plot of mercury injection data. Φ=13.07 %, *Re*=98.43 %, *k*=12.981 md, mean pore throat size=14.15 phi; B—Plot of mercury saturation/capillary pressure versus mercury saturation

*1. ábra.* A—A higanyinjekciós adatok log-log hiperbolikus ábrázolása Φ=13,07 %, *Re*=98,43 %, *k*=12,981 md, átlagos pórusnyílás méret=14,15 phi; B—A higanytelítettség/kapilláris nyomás ábrázolása a higanytelítettség függvényében

*Рис.1.* А–Гиперболическое изображение данных нагнетания ртути в логарифмическом масштабе. Φ=13,07 %, *Re* =98,43 %, *k* =12,981 md, средний размер отверстия пор=14,15phi; В–Зависимость отношения насыщенности ртутью и капиллярного давления от насыщенности ртутью

## 3. Analysis of apex

The distribution of mercury saturation (*Fig. 1B*) reveals two major apexes ($r_{36}$ and $r_{50}$) that are generally present and characterize the sandstones of the Törtel Formation. The most predominant apex is the $r_{50}$. These apexes are defined as the pore aperture sizes corresponding to the mercury saturation of 36 % and 50 % respectively. Although PITTMAN [1992] pointed out that the mean apex calculated for 196 sandstone samples had a mercury saturation of 36 % ($r_{36}$), the calculated apex ($r_{50}$) proves that this latter is appropriate and convenient for sandstones of the Törtel Formation. This is confirmed by the relationships between the pore aperture radii ($r_{36}$, $r_{50}$) and the rock porosity (*Figs. 2A* and *2B*).

Based on regression analysis with *r* (apex) as the dependant variable, the relationship between the pore aperture size corresponding to the apex ($r_{36}$ in Å) and porosity (Φ in %) is:

$$r_{36} = 466.82\, e^{0.193\Phi} \qquad (4)$$

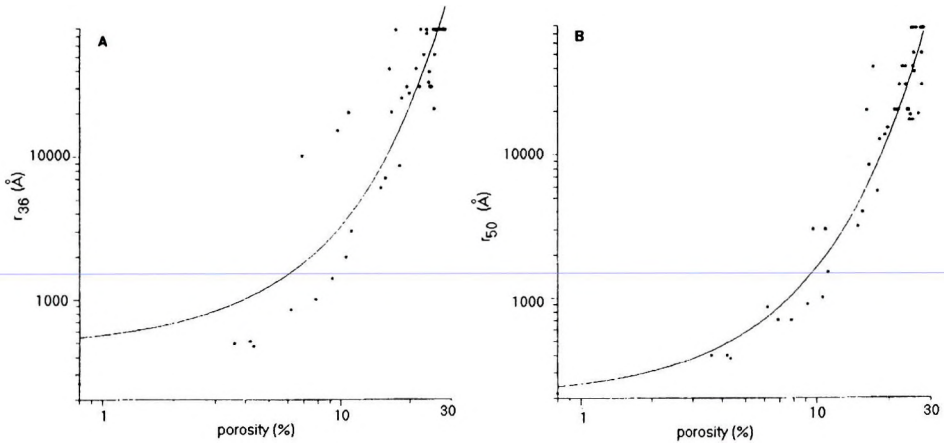


*Fig. 2.* Pore aperture radii versus porosity. A—$r_{36}$; B—$r_{50}$
*2. ábra.* Pórusnyílás sugarak a porozitás függvényében. A—$r_{36}$; B—$r_{50}$
*Рис. 2.* Зависимость радиуса отверстия пор от пористости. А—$r_{36}$; В—$r_{50}$

This equation yields a correlation coefficient of 0.901. On the other hand, the relationship (Fig. 2B) considering $r_{50}$ as the mean apex characterizing the sandstone of the Törtel Formation is:

$$r_{50} = 203.97\, e^{0.207\Phi} \tag{5}$$

This equation is characterized by a high correlation coefficient (0.96).

Uncorrected gas permeability is plotted against both of $r_{36}$ and $r_{50}$ (*Figs. 3A and 3B*). These relationships were characterized by slightly low correlation coefficients (0.54 and 0.62 respectively). The regression equations representing these relations are:

$$r_{36} = 2277.5\, K^{0.542} \tag{6}$$

$$r_{50} = 993.5\, K^{0.61} \tag{7}$$

where $K$ is the gas permeability (md).

Results showed that there is a favourable comparison with either $r_{36}$ or $r_{50}$. However, results obtained with $r_{36}$ are somewhat optimistic (*Fig. 4*) especially in sandstones of the Törtel Formation. An examination of 12 nonproductive wells in the Algyő field using both $r_{36}$ and $r_{50}$ gave complete agreement for 10 dry wells (83.3 %), while they have a pore aperture size $< 0.5$ μm ( 5000 Å). Another examination of 33 producing wells in the Algyő field indicated that $r_{50}$ gives 100 % reliable results; $r_{36}$ gave 95 % reliable results. Therefore $r_{50}$ could be considered as the most effective tool for distinguishing nonproductive from productive wells in respect of the lithological traps of the Törtel Formation in the Great Hungarian Plane.

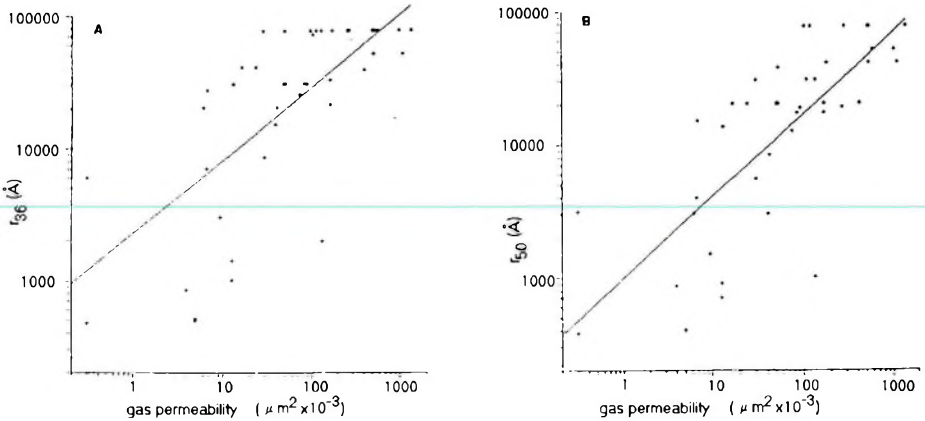


*Fig. 3.* Pore aperture radii versus gas permeability. A—$r_{36}$; B—$r_{50}$
*3. ábra.* Pórusnyílás sugarak a gáz permeabilitás függvényében. A—$r_{36}$; B—$r_{50}$
*Рис. 3.* Зависимость радиуса отверстия пор от проницаемости газа. А—$r_{36}$; В—$r_{50}$

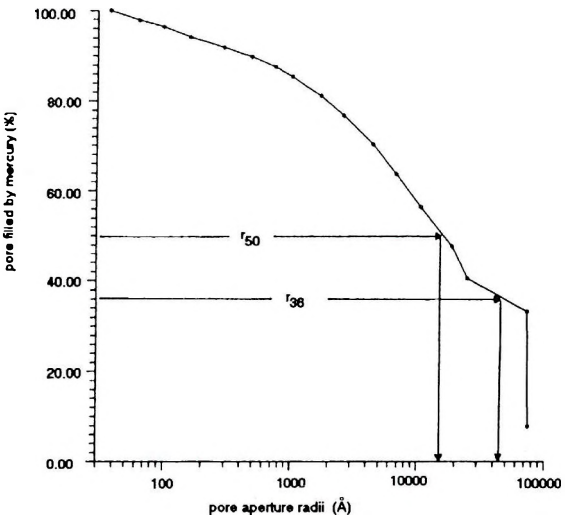


*Fig. 4.* Semilog mercury injection plot with pore aperture size plotted on the logarithmic axis. Φ=12.38 %, $k$=6.38 md
*4. ábra.* Higanyinjektálás ábrázolása féllogaritmikus rendszerben, a pórusnyílás méret a logaritmikus tengelyen ábrázolva. Φ=12,38 %, $k$=6,38 md
*Рис. 4.* Изображение нагнетания ртути в полулогарифмическом масштабе. Размер пор изображен в логарифмическом масштабе. Φ=12,38 %, $k$=6,38 md

## 4. Displacement pressure

A relationship between the displacement pressure measured graphically on the capillary pressure-mercury injection curve [SCHOWALTER 1979] and porosity is shown in *Fig. 5A*. The relationship is represented by regression line equation:

$$\Phi = 30.5\ Pd^{-0.312} \tag{8}$$

where *Pd* is the displacement pressure (psia).

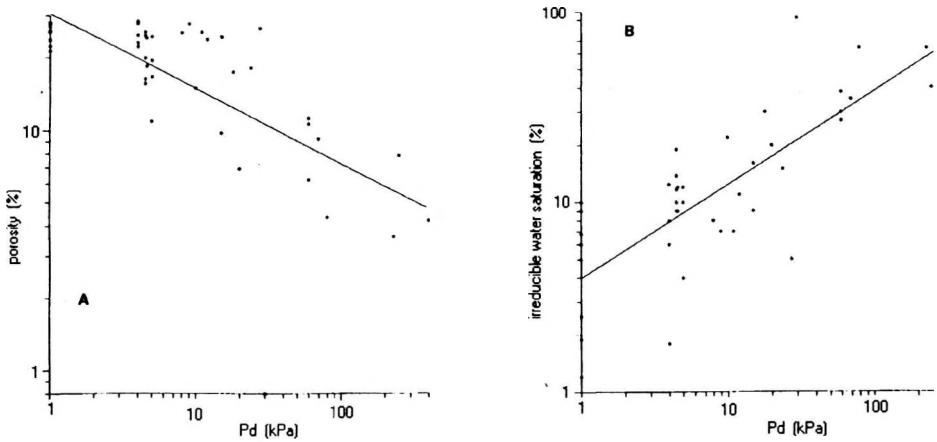


*Fig. 5.* Porosity (A) and irreducible water saturation (B) versus displacement pressure
*5. ábra.* Porozitás (A) és nem redukálható víztelítettség (B) az elmozdulási nyomás függvényében
*Рис.5.* Зависимость пористости (А) и остаточной водонасыщенности (В) от давления смещения

This equation has a correlation coefficient of -0.85. *Fig. 5B* exhibits a relationship berween the irreducible water saturation calculated from capillary pressure curves and the displacement pressure. This relationship is provided with a reliable correlation coefficient (0.81) governing the equation:

$$S_{wir} = 3.99\ Pd^{0.49} \tag{9}$$

where $S_{wir}$ is the irreducible water saturation (%).

Hence, the displacement pressure could be estimated from the measured rock porosity which usually obtained during the conventional core analysis.

## 5. Recovery efficiency

EL-SAYED [1988] studied the recovery efficiency of 27 sandstone core samples obtained from the Algyő-2 reservoir formation of the Algyő field. He concluded that the recovery efficiency of these deposits is influenced mainly by tortuosity and matrix conductivity, or tortuosity and permeability per porosity ratio.

*Figure 6A* reveals a negative relationship between mercury recovery efficiency and rock porosity of sandstones of the Törtel Formation. In some cases — especially in carbonate reservoirs (e.g. limestones and dolomites) — positive relations have been recorded in dolostones [WARDLAW 1976 and 1980] and in oolitic limestones of Jurassic age [MELAS, FRIEDMAN 1992]. This phenomenon depends mainly on the wettability of mineral grains forming the rock-pore network. The obtained relationship (Fig. 6A) is presented by the regression line equation:

$$Re = 106.86 - 1.62\Phi \qquad (10)$$

where *Re* is the mercury recovery efficiency (%) and Φ is the porosity (%).

This equation is characterized by a correlation coefficient of -0.7. It is worth mentioning that an insignificant correlation coefficient has been obtained for the relation between mercury recovery efficiency and gas permeability.

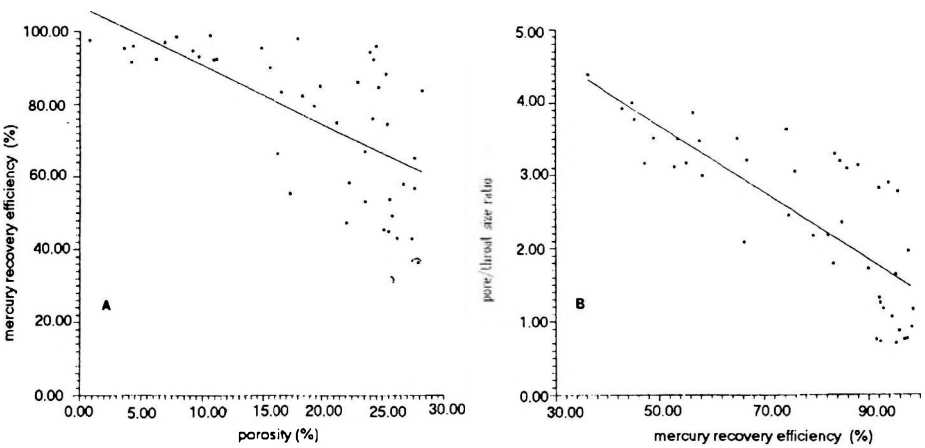


*Fig. 6.* Mercury recovery efficiency versus porosity (A) and pore/throat size ratio (B)

*6. ábra.* Higany visszanyerési hatékonyság a porozitás (A) és pórus/nyílásméret arány függvényében

*Рис. 6.* Зависимость эффективности извлечения ртути от пористости (А) и от отношения размера пор и отверстий (В)

Therefore, rock porosity from routine core analysis could be used for delineating the oil recovery efficiency in the sandstones of the Törtel Formation.

The calculated mercury recovery efficiency is plotted against the pore/throat size ratio (*Fig. 6B*). The graph displays a negative relationship, while recovery efficiency decreases with increasing pore/throat size ratio. This is completely consistent with the relations introduced by WARDLAW and CASSAN [1979]. The calculated average pore/throat size ratio for the sandstones of the Törtel Formation was found to be 2.7, while the mean pore throat size was measured by phi units. This average value, when plotted on the graph of Fig. 6B, gives a mercury recovery efficiency of around 70 %.

## 6. Conclusions

Porosity and permeability of sandstones of the Törtel Formation, from routine core analysis could be used to estimate various reservoir parameters derived from mercury injection.

Among 45 sandstone core samples, the mean apex of log-log mercury injection plots was at a mercury saturation of 50 %.

The apex of mercury saturation distribution exhibits bimodal type ($r_{36}$ and $r_{50}$). The empirically derived relationships between porosity and the pore aperture radii of $r_{36}$ and $r_{50}$ are presented by Eqs. (4) and (5). They are reliable enough for estimating the apexes and then for delineating the productive and nonproductive wells in this trap.

Displacement pressure derived from mercury injection tests could be estimated from either porosity or irreducible water saturation data by using empirical equations (Eqs. 8 and 9). Although mercury recovery efficiency reveals negative relationships with both porosity and pore/throat ratio, it could be estimated from rock porosity using the calculated empirical equation (Eq. 10).

## Acknowledgements

This work was supported by the Hungarian Hydrocarbon Institute (SZKFI) during 1991 on the basis of a consultation contract. I wish to thank this organization for its financial support. Special thank is due to Dr. László VOLL, vice president; Dr. E. BALÁZS, Dr. K. SZENTGYÖRGYI, Dr. I. RÉVÉSZ, Dr. J. GEIGER, Mrs J. KOMLÓSI and Mr. B. KISS of the Geology Department and sedimentological team in both Budapest and Szeged for their continuous help. I also wish to thank Dr. Á. BÁN, former vice president of the Hungarian Hydrocarbon Institute, for fruitful discussions.

## REFERENCES

BÁN Á., EL-SAYED A. M. A. 1987: Genetic delineation of deltaic rock types in terms of log curve shape in the Algyő-2 hydrocarbon reservoir, Hungary. Acta Geol. Hung. **30**, 1-2, pp. 231-240

BÉRZCI I., PHILLIPS R. L. 1985: Processes and depositional environments within Neogene deltaic-lacustrine sediments, Pannonian Basin, Southeast, Hungary. Geophysical Transactions **31**, 1-3, pp. 55-74

BERG R. R. 1975: Capillary pressure in stratigraphic traps. AAPG Bulletin **59**, pp. 939-956

EL-SAYED A. M. A. 1981: Geological and petrophysical studies for the Algyő-2 reservoir evaluation, Algyő oil and gas field, Hungary. Ph.D. thesis, Hungarian Academy of Sciences, Budapest, p. 166

EL-SAYED A. M. A. 1983: Skewness-kurtosis crossplot of pore throat size distribution as a discriminating factor for deltaic rock genetic types. 2nd Ann. Mtg., Egyptian Geophys. Soc., pp. 75-85

EL-SAYED A. M. A. 1988: Statistical relationships among some petrophysical parameters for Algyő-2 sandstone, Hungary. Geophys. Res. Bull. (National Geophys. Res. Inst. India) **26**, 3, pp. 96-102

EL-SAYED A. M. A. 1991: Reservoir characteristics of the Upper Pannonian hydrocarbon reservoirs in the Algyő field, Hungary. Internal report of the Hungarian Hydrocarbon Institute (SZKFI), p. 47

EL-SAYED A. M. A., VOLL L. 1992: Empirical prediction of porosity and permeability in deltaic sandstones of the Törtel Formation, Hungary. Scientific Bulletin, Ain Shams Univ., **30**, pp. 461-487

HUTCHEON I., OLDERSHAW A. 1985: The effect of hydrothermal reactions on the petrophysical properties of carbonate rocks. Can. Pet. Geol. Bull. **33**, pp. 359-377

JUHÁSZ GY. 1991: Lithostratigraphical and sedimentological framework of the Pannonian (s.l.) sedimentary sequence in the Hungarian Plain (Alföld), Eastern Hungary. Acta Geol. Hung. **34**, 1-2, pp. 53-72

KOPASKA-MERKEL D. C., FRIEDMAN G. M. 1989: Petrofacies Analysis of Carbonate Rocks: example from Lower Paleozoic Hunton Group of Oklahoma and Texas. AAPG Bulletin **73**, 11, pp. 1289-1306

MAGARA K. 1978: Geological model predicting optimum sandstone percent for oil accumulation. Can. Pet. Geol. Bull. **26**, pp. 380-388

MELAS F. F., FRIEDMAN G. M. 1992: Petrophysical characteristics of the Jurassic Smackover Formation, Jay field, Conecuh embayment, Alabama and Florida. AAPG Bulletin, **76**, 1, pp. 81-100

MORAES M. A. S. 1991: Diagenesis and microscopic heterogeneity of lacustrine deltaic and turbiditic sandstone reservoirs (Lower Cretaceous), Potiguar Basin, Brazil. AAPG Bulletin, **75**, pp.1758-1771

MUCSI M., RÉVÉSZ I. 1975: Neogene evolution of the south-eastern part of the Great Hungarian Plain on the basis sedimentological investigations. Acta Mineral. Petrograph. **22**, 1, pp. 29-49

PITTMAN E. D. 1989: Nature of the Terry sandstone reservoir, Spindle Field, Colorado. *In*: Coalson E. B. (ed.), Petrogenesis and petrophysics of selected sandstone reservoirs of the Rocky Mountain region. Rocky Mount. Assoc. of Geol., Denver, Colorado, pp. 245-254

PITTMAN E. D. 1992: Relationship of porosity and permeability to various parameters derived from mercury injection-capillary pressure curves for sandstones. AAPG Bulletin **76**, 2, pp. 191-198

SCHOWALTER T. T. 1979: Mechanics of secondary hydrocarbon migration and entrapment. AAPG Bulletin **63**, pp. 723-760

SOMFAI A. 1976: Classification of hydrocarbon trap types on the area of the Pannonian Basin (within Hungary) and possibilities of the investigation of lithological and stratigraphical trap types. (in Hungarian) Földtani Kutatás **19**, 4, pp. 11-18

STOODLY K. D. C. 1984: Applied and computational statistics—a first course. Ellis Horwood, New York

SWANSON B. F. 1977: Visualizing pores and non-wetting phase in porous rocks. Ann. Fall. Res. Conf., Soc. Pet. Engs., No. **6857**, p. 10

SWANSON B. F. 1981: A simple correlation between permeabilities and mercury capillary pressures. J. Pet. Technol., 1981 Dec., pp. 2498-2504

THOMEER J. H. M. 1960: Introduction of a pore geometrical factor defined by the capillary pressure curve. J. Pet. Technol., 1960 March, pp. 73-77

WARDLAW N. C. 1976: Pore geometry of carbonate rocks as revealed by pore casts and capillary pressure. AAPG Bulletin **60**, pp. 245-257

WARDLAW N. C., CASSAN J. P. 1979: Oil recovery efficiency and the rock pore properties of some sandstone reservoirs. Can. Pet. Geol. Bull. **27**, pp. 117-138

WARDLAW N. C. 1980: The effect of pore structure on displacement efficiency in reservoir rocks and in glass micromodels. SPE Paper, Soc. Pet. Engs., No. **8843**, pp. 345-352

WASHBURN E. W. 1921: Note on a method of determining the distribution of pore sizes in a porous materials. Proc. National Acad. Sci., USA, **7**, pp. 115-116

SI Metric conversion factors:

psi · 6.894 575 E+03 = MPa
dyn · 1.0 E-05 = N
md · 9.869 233 E-04 = $mm^2$
phi unit = $-\log_2 S$, where S is diameter in mm

## POROZITÁS ÉS PERMEABILITÁS KAPCSOLATA HIGANYINJEKTÁLÁSBÓL SZÁRMAZTATOTT PARAMÉTEREKKEL, A TÖRTEL FORMÁCIÓ HOMOKKÖVEIRE

Abdel Moktader A. EL-SAYED

A higanyinjektálás-kapilláris nyomás vizsgálatok költségesek, ezért alkalmazásuk nem terjedt el széles körben, bár a belőlük levezetett paraméterek mind tározó-geológiai, mind mérnöki szempontból értékesek. A higanyinjektálásos tesztekből becsült pórusnyílás méret adatokat a sztratigráfiai szénhidrogén csapdák zárórétegeinek kiértékelésére használtuk. A Törtel formációból származó (Algyő gáz- és olajmező), 45 homokkő magminta higanyinjektálás-kapilláris nyomás görbéit vizsgáltuk.

A tanulmány empírikus egyenleteket vezet le a pórusnyílás méretre és néhány fontos tározó paraméterre mindennapos magminta-analízis eljárásokból (porozitás és/vagy permeabilitás). Az $r_{36}$ és $r_{50}$ pórusnyílás méreteket becsültük, mely alapján az $r_{50}$ méret tűnik a legjelentősebbnek és leghatékonyabbnak a Törtel formáció homokköveiben lévő szénhidrogén csapdák leírására. Ezen kívül a higanyvisszanyerési együttható becslését is elvégeztük.

# СВЯЗЬ ПОРИСТОСТИ И ПРОНИЦАЕМОСТИ С ПАРАМЕТРАМИ ВЫВЕДЕННЫМИ ПО НАГНЕТАНИЮ РТУТИ ДЛЯ ПЕСЧАНИКОВ ТЕРТЕЛЬСКОЙ ФОРМАЦИИ

Абдел Моктадер А. ЭЛЬ-САЕД

Исследование капиллярного давления при нагнетании ртути является дорогостоящим методом, поэтому он не получил широкого применения, несмотря на ценность получаемых данных как и для геологии резервуаров, так и с инженерной точки зрения. Размер отверстия пор, оцененный по таким исследованиям, применяли для описания закрывающих пластов стратиграфических резервуаров. Были проанализированы кривые нагнетание ртути-капиллярное давление по 45 кэрновым пробам песчаников Тертельской Формации месторождения нефти и газа Альде.

В статье выведены эмпирические уравнения для расчета размера отверстияпор и некоторых важных параметров резервуаров по данным стандартного анализа кэрновых проб (пористость и/или проницаемость). Размеры отверстия пор $r_{36}$ и $r_{50}$ получены путем оценки. Самым значительным является размер $r_{50}$, который наиболее эффективно применяется для описания резервуаров Тертельской формации. Также выполнена оценка коэффициента извлечения ртути.

GEOPHYSICAL TRANSACTIONS 1993
Vol. 38. No. 1. pp. 47-53

# ANALYSIS OF GRAVITY ANOMALIES DUE TO CYLINDRICAL STRUCTURES WITH LINEARLY VARYING DENSITY

A. V. VARAPRASADA RAO*, G. SAHADEV**, P. SRINIVASA RAO** and N. SUNDARARAJAN**

Gravity anomalies $g(x)$ due to 2-D cylindrical structures with linearly varying density and the corresponding quadratic function $H(x)$ are analysed to determine the depth ($Z$) of the centre of the cylinder, the radius ($R$) and the rate of change of density contrast ($a$). The abscissa of the point of intersection of $g(x)$ and $H(x)$ yields the approximate value of $Z$ and thereby the depth is obtained with better accuracy by Newton-Raphson's iterative process.

**Keywords: gravity anomaly, cylindrical model, Hilbert transform**

## 1. Introduction

Interpretation of geophysical anomalies is generally carried out by attributing regular geometrical shapes to the structures which generate the anomalous field. While doing so, particularly in gravity interpretation, the density contrast is assumed to be uniform. At times this assumption is inappropriate since the density of the sedimentary rocks increases with depth, hence any anomalous body surrounded by them shows a decrease in its density contrast with depth when its density remains unchanged throughout its volume [MURTHY, RAO 1979]. It is also reported that the density increases exponentially with depth in some cases [CORDELL 1973]. Therefore it is reasonable to conclude that the density contrast varies linearly in depth for sources at

* Presently with the Department of Computer Sciences, Indian Inst. of Tech., New Delhi-110 016, India

** Centre of Exploration Geophysics, Osmania University, Hyderabad-500 007, India

Manuscript received (revised version): 10 July, 1991

moderate depth and exponentially in the case of shallow structures. The non-uniformity in density contrast is primarily due to the compaction of sedimentary strata that overlie the basement.

Some authors have made attempts to interpret gravity anomalies by means of bodies with non-uniform density [BHATTACHARYYA, CHAN 1977, MURTHY, RAO 1979, MOHAN et al. 1977]. These methods either turned out to be cumbersome or require certain assumptions to enable the analysis to be carried out. The limit of the spectral analysis [MOHAN et al. 1977] of such gravity anomalies is that it is suitable only for relatively lengthy profiles.

Application of the Hilbert transformation for interpreting gravity anomalies is known from the literature [GREEN 1976, SUNDARARAJAN et al. 1983 and 1987]. In these methods the parameters of the causative bodies are obtained by simple mathematical expressions involving the gravity field and its Hilbert transform. Even for short profiles the method of Hilbert transform ensures reliable results [SUNDARARAJAN 1982].

Herein we present a method for interpreting gravity anomalies due to cylindrical structures with variable density. The method is illustrated with a theoretical model.

## 2. Theory

*Figure 1a* illustrates the geometrical configuration of a horizontal circular cylinder. Assuming the density contrast at the apex of the cylinder to be ($\sigma$) and the rate of change of the density contrast ($a$) varying linearly with depth ($z$), the gravity effect due to the cylinder in such a case is given as [MURTHY 1973]:

$$g(x) = A \frac{z}{x^2 + z^2} - B \frac{z^2 - x^2}{(x^2 + z^2)^2} \tag{1}$$

where

$$A = 2 \pi f R^2 (\sigma + a R) \tag{2}$$

$$B = \pi f a R^4/2 \tag{3}$$

and $f$ is the universal gravitational constant.

The Fourier transform of $g(x)$ is given as [MOHAN et al. 1977]:

$$F(\omega) = \pi e^{\omega z} (A - B\omega) \ . \tag{4}$$

Here, the Fourier transform consists of only the real part, as $g(x)$ is an even function. In this case, the equation of Hilbert transforms is reduced to [SUNDARARAJAN et al. 1983]:

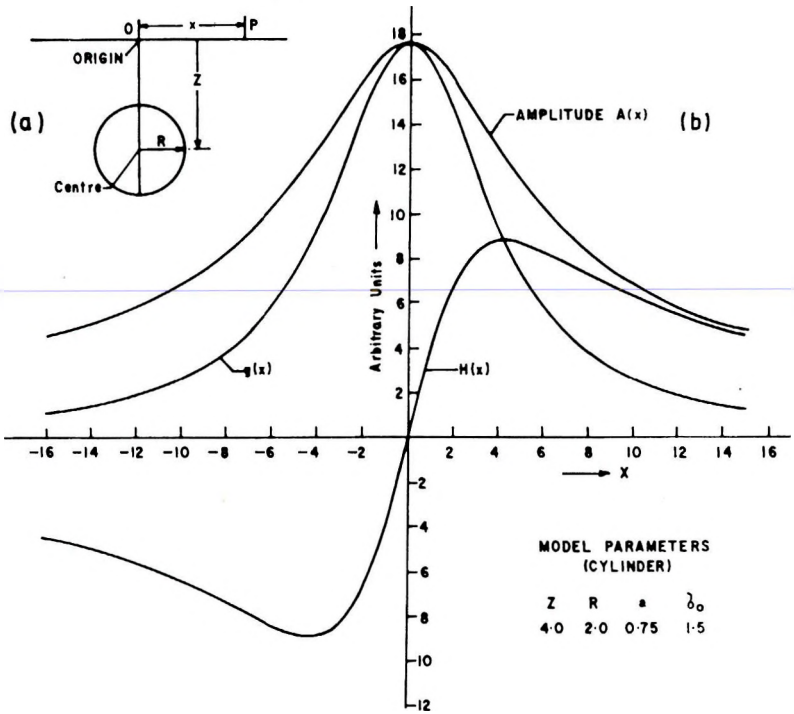


*Fig. 1.* a) Geometry of a horizontal circular cylinder; b) Gravity effect $g(x)$ due to cylindrical structure, the Hilbert transform $H(x)$ and the amplitude $A(x)$

*1. ábra.* a) A horizontális hengermodell geometriai vázlata; b) A hengeres szerkezet gravitációs hatása $g(x)$, ennek Hilbert transzformáltja $H(x)$ és az amplitúdó függvény $A(x)$

*Рис. 1.* а) Геометрическая модель горизонтального цилиндра; b) Аномалия силы тяжести $g(x)$ цилиндрической структуры, трансформант Гилберта $H(x)$ и амплитудная функция $A(x)$

$$H(x) = \frac{-1}{\pi} \int_0^{\infty} \mathrm{Re}\, F(\omega) \sin(\omega x)\, d\omega \,. \tag{5}$$

Equations (4) and (5) yield the Hilbert transform of $g(x)$ as:

$$H(x) = A \frac{x}{(x^2 + z^2)} - B \frac{2xz}{(x^2 + z^2)^2} \,. \tag{6}$$

The Hilbert transform of $g(x)$ can also be computed by the convolution process as:

$$H(x) = \frac{1}{\pi x} * g(x)$$

where $*$ denotes the convolution. In the above convolution representation $g(x)$ can be replaced by its horizontal derivative of any order and therefore the resulting Hilbert transform would be the vertical derivative of the corresponding order.

## 3. Analysis

The origin, which is a prerequisite and is of paramount importance in interpreting potential field anomalies, is identified from the maximum of the amplitude defined by the equation:

$$A(x) = \sqrt{g(x)^2 + H(x)^2} \quad . \tag{7}$$

The first order vertical derivative of the gravity effect $g(x)$ is obtained by differentiating Eq. (1) with respect to $z$ as:

$$g_z(x) = \frac{A\,(x^2 - z^2)}{(x^2 + z^2)^2} + \frac{2Bz\,(z^2 - 3x^2)}{(x^2 + z^2)^3} \quad . \tag{8}$$

At $x = 0$ and $z = Z$, Eqs. (1) and (8) reduce to

$$g(0) = A/Z - B/Z^2 \tag{9}$$

$$g_z(0) = -A/Z^2 + 2B/Z^3 \quad . \tag{10}$$

Constants $A$ and $B$ can be evaluated from Eqs. (9) and (10) as:

$$A = 2\,g(0)\,Z + g_z(0)\,Z^2 \tag{11}$$

$$B = g(0)\,Z^2 + g_z(0)\,Z^3 \quad . \tag{12}$$

At the abscissa of the point of intersection of $g(x)$ and $H(x)$ we have $g(x) = H(x)$ at $x = x_1$, that is:

$$A\,(Z - x_1)\,(x_1^2 + Z^2) = B\,(Z^2 - x_1^2 - 2\,Z\,x_1). \tag{13}$$

Eliminating $A$ and $B$ from Eq. (13) with the help of Eqs. (11) and (12), we obtain a cubic equation in $Z$ as:

$$K\,Z^3 + L\,Z^2 + M\,Z + N = 0 \tag{14}$$

where,

$$K = g(0) + x_1\,g_z(0)$$
$$L = 2\,g_z(0)\,x_1^2$$
$$M = 3\,g(0)\,x_1^2 - g_z(0)\,x_1^3$$
$$N = -2\,g(0)\,x_1^3$$

Equation (13) can be solved for $Z$ using the Newton-Raphson's method, treating $x_1$ as the approximate root [VARAPRASADA RAO 1988].

From Eqs. (2) and (3), the radius of the cylinder is obtained as a cubic equation in $R$ as:

$$R^3 - AR\,/\,(2\,\pi\,f\,\sigma) + 2B\,/(\pi\,f\,\sigma) = 0 \quad . \tag{15}$$

Using Cardon's method Eq. (14) can be solved for $R$ assuming the value of $\sigma$.

Finally the rate of change of density $a$ is obtained from Eq. (2) as:

$$a = \frac{A - 2\pi f \sigma R^2}{2\pi f R^3} \quad . \tag{16}$$

Thus the following parameters, viz. the depth ($Z$), the radius ($R$) and the rate of change of density ($a$) are evaluated.

## 4. Theoretical example

The application of the procedure detailed in the text is demonstrated by a synthetic model with a set of parameters, namely: $Z$=4.0, $R$ =2.0, $a$=0.75 and $\sigma$=1.5 (all in arbitrary units). The gravity effect due to the cylinder, its Hilbert transform and the amplitude curve are computed and shown in Fig. 1b. Using the procedure detailed above, the parameters are evaluated as: $Z$=3.995, $R$=2.00 and $a$=0.75 (all in arbitrary units). Thus the assumed and evaluated values are in good agreement with each other and thereby substantiate the validity of the method.

## 5. Discussion

The computation of the Hilbert transform of the discrete gravity data can be carried out either through the frequency domain using the fast Fourier transforms (FFT) algorithm or in the time/space domain using the convolution process.

The discrete Hilbert transform (DHT) via the frequency domain can be expressed as [MOHAN et al. 1982]:

$$H(m\,\Delta x) = \frac{1}{\pi} \sum_{n=0}^{N/2-1} g(m\,\Delta x)\, e^{-i\,n\,\omega_0\,m\,\Delta x} \quad . \tag{17}$$

On the other hand the digital form of the convolution process can be expressed as [TANER et al. 1979]:

$$H(x) = \frac{2}{\pi} \sum_{n=-\infty}^{\infty} g\,(n\,\Delta x)\, \frac{\sin^2 (n\pi/2)}{n} \tag{18}$$

where

$\Delta x$— is the sampling interval

$\omega_0$—is the fundamental frequencs given as $\omega_0 = 2\pi/n\Delta x$

$N$ — is the total number of samples.

Basically both Eqs. (17) and (18) give the same results. However the computation in the frequency domain is much faster than the time domain digital convolution process. In using Eq. (17), the number of samples $n$ needs to be $2^k$ where $k$ is a positive integer whereas this it is not the case with the convolution process.

The stability of the vertical derivative in such an interpretation has been studied by one of the authors [SUNDARARAJAN et al. 1990] and it was found that the effectiveness of the interpretation is only slightly diminished in the presence of a noise level as high as 50 %.

If $a$=0, i.e. for a homogeneous body, $Z$ can also be evaluated by a simple division of Eq. (10) by Eq. (9) as:

$$Z = g_z(0) / g(0) \quad . \tag{19}$$

This perhaps appears to be simpler than the use of Newton-Raphson's method.

## REFERENCES

BHATTACHARYYA B. K., CHAN K. C. 1977: Computation of gravity and magnetic anomalies due to inhomogeneous distribution of magnetization and density in a localized region. Geophysics **42**, 3, pp. 602-609

CORDELL L. 1973: Gravity analysis using an exponential density-depth function — San Jacinto Graben, California. Geophysics **38**, 4, pp. 684-690

GREEN R. 1976: Accurate determination of the dip angle of a geological contact using a gravity method. Geophysical Prospecting **24**, 2, pp. 265-272

MOHAN N. L., SESHAGIRI RAO S. V., BHIMASANKARAM V. L. S. 1977: Analysis of the gravity effect due to horizontal circular cylinder with variable density. Curr. Sci. **46**, 12, pp. 404-405

MOHAN N. L., SUNDARARAJAN N., SESHAGIRI RAO S. V. 1982: Interpretation of some 2-D magnetic bodies using the Hilbert transform. Geophysics **47**, 3, pp. 376-387

MURTHY, I.V. R. 1973: Gravitational attraction of a horizontal circular cylinder with the density contrast varying linearly with depth. (in Italian) Bolletino dell Associazione Geofisica Italiana, **22**, 5-6, p. 407.

MURTHY I.V. R., RAO B. D. 1979: Gravity anomalies of two-dimensional bodies of irregular cross-section with density contrast varying with depth. Geophysics **44**, 9, pp. 1525-1530

SUNDARARAJAN N. 1982: Interpretation techniques in exploration geophysics using Hilbert transform. Ph.D. thesis, Osmania University, Hyderabad, India

SUNDARARAJAN N., MOHAN N. L., SESHAGIRI RAO S. V. 1983: Gravity interpretation of two dimensional fault structures using Hilbert transform. J. of Geophys. **53**, 1, pp. 34-41

SUNDARARAJAN N., ARUN KUMAR I., MOHAN N. L. 1987: Analysis of gravity gradient over a thin infinite sheet. Proc. of Indian Acad. of Sci. (Earth and Planetary Sciences) **96**, pp. 11-14

SUNDARARAJAN N., ARUN KUMAR I., MOHAN N. L., SESHAGIRI RAO S. V. 1990: Use of the Hilbert transform to interpret self-potential anomalies due to two-dimensional inclined sheets. Pure Appl. Geophys. **133**, 1, pp. 117-126

TANER M. T., KOEHLER F., SHERIFF R. E. 1979: Complex seismic trace analysis. Geophysics **44**, 6, pp. 1041-1063

VARAPRASADA RAO A. V. 1988: Analysis of the gravity anomalies due to cylindrical structures with linearly varying density. M.Sc (Tech.) Project work, subm. to the Centre of Exploration Geophysics, Osmania University

## LINEÁRISAN VÁLTOZÓ SŰRŰSÉGŰ HENGERES SZERKEZETEK GRAVITÁCIÓS ANOMÁLIÁINAK VIZSGÁLATA

A. V. VARAPRASADA RAO, G. SAHADEV, P. SRINIVASA RAO és N. SUNDARARAJAN

Lineárisan változó sűrűségű kétdimenziós hengeres szerkezetek által okozott gravitációs anomáliákat $g(x)$ és az ennek megfelelő $H(x)$ másodfokú függvényt vizsgálja a dolgozat, a hengeres szerkezet középpontjának mélysége ($Z$), sugara ($R$), valamint a sűrűségkontraszt változási arányának ($a$) meghatározására. A $g(x)$ és $H(x)$ függvények metszéspontjának abszcisszatengelyen felvett értékéből a mélység ($Z$) közelítő értéke határozható meg, így ezen paraméter a Newton-Raphson iteratív eljárással nagyobb pontossággal számítható.

## ИССЛЕДОВАНИЕ АНОМАЛИЙ СИЛЫ ТЯЖЕСТИ ОТ ЦИЛИНДРИЧЕСКИХ СТРУКТУР ПРИ ЛИНЕЙНО ИЗМЕНЯЮЩЕЙСЯ ПЛОТНОСТИ

А. В. ВАРАПРАСАДА РАО, Г. САХАДЕВ, П. СРИНИВАСА РАО и Н. СУНДАРАРАДЖАН

В статье исследуются аномалии силы тяжести $g(x)$ двухмерных цилиндрических структур с линейно изменяющейся плотностью и соответствующие им функции второй степени $H(x)$ с целью определения глубины залегания центра ($Z$) и радиуса ($R$) цилиндрической структуры, а также коэффициента изменения избыточной плотности ($a$). По абсциссе точки пересечения функций $g(x)$ и $H(x)$ определяется приблизительная глубина ($Z$) с большей точностью, чем с методом Ньютона-Рафсона.

GEOPHYSICAL TRANSACTIONS 1993
Vol. 38. No. 1 pp. 55- 66

# INTERPRETATION PROBLEMS OF ELECTRIC SOUNDING AND PROFILING IN REGIONS OF COMPLICATED GEOLOGY AND RUGGED TERRAIN

Alfred FRASHËRI*

Electric soundings in zones of complicated geology and rugged terrain (e.g. in the folded mountainous belt of the Albanids), have shown the existence of electric field scattering. The lateral changes of resistivity, the limited extension of geologic structures, the existence of several structures close to each other, and rugged terrain are characteristic features of this complicated geoelectrical medium.

Electric field scattering distorts the apparent resistivity values; if the apparent resistivity curves were interpreted without regard to the above phenomena and without performing correction for their effect, an unreliable view would be taken. Therefore the electric field scattering of the direct current was studied in a heterogeneous medium with curved boundaries and in rugged terrain. Potential response was computed with the aid of the quasi-harmonic equation (two- and three-dimensional) for boundary conditions of Neumann type. To solve the quasi-harmonic equation in a trapezoidal zone, in the lower half-space it was replaced by the corresponding variational problem, which can be solved by the finite-element method, giving an approximate representation of the electric field scattering. We have developed two computer programs in Fortran programming language for 2-D and 3-D modelling.

Results of some geoelectric models are given. In these models the electrical soundings are taken over the interface of different types of rocks and flexures, or above horsts and grabens. The programs are also used to correct different effects, including terrain effects.

**Keywords: electric sounding, Albania, resistivity, finite-element analysis**

## 1. Introduction

The widespread use of shallow electric soundings for engineering studies and in mineral prospecting and the use of deep electrical soundings in the search

* Polytechnic University of Tirana, Faculty of Geology and Mining, Tirana, Albania

Manuscript received (revised version): 10 October, 1991

for oil and gas, have brought forth some problems related to the interpretation of the electric soundings in cases of complicated geology and rugged terrain in some regions of Albania. The experience gained and the theoretical analysis of the phenomena observed create possibilities for their solution and the overcoming of their influence.

Electric soundings are interpreted by comparing them with theoretical models of simplified geoelectrical sections (horizontal, sometimes inclined layers which are always flat and have infinite extent, without horizontal changes of the resistivity). In practice the use of electric sounding involves a number of aspects related to the surface geology and terrain:

— the relief is rugged in many areas;
— lateral (abrupt or gradual) changes of resistivity exist due to the presence of different types of rocks. The contact between them may be outcropped or may be covered by overburden;
— the geological structures have smaller extent than their depth, so the geoelectric boundaries are limited;
— various types of geological structures are often situated close to each other, at the same or different depths.

The above mentioned factors influence the scattering of the electric field and consequently the values of the apparent resistivity measured during the electric soundings.

## 2. Terrain effect in resistivity surveys

Rugged terrain causes deformations on the sounding and the resistivity profiles [DAHNOV 1953, KOEFOED 1979, FRASHËRI et al. 1984] due to the changes of the subsurface current distribution. For example when the current line configuration is perpendicular to the strike of a crest, the apparent resistivity at first begins to decrease, because of the decrease of the current density in the region where the potential electrodes are placed. The opposite is the case when the centre of the sounding is located over a valley. A more complicated influence appears on the resistivity curve when the centre of the sounding is located over the foot, or a crest, or over the side of a valley. If these deformations are not taken into consideration they may lead to a wrong interpretation. Evaluation of terrain effects can be made in two ways: firstly, taking into consideration not only the sounding to be interpreted but the neighbouring curves as well. At the same time information about the resistivity of the outcropped rocks in the sounding area must be provided. Secondly, correction of apparent resistivity with respect to the terrain effects is carried out.

For terrain correction we use the finite-element method to solve numerically the Laplace's equation in order to study the electric field behavior in a heterogeneous medium with curved boundaries of any configuration (*Fig. 1*). The finite-element modelling procedures are treated mathematically in several

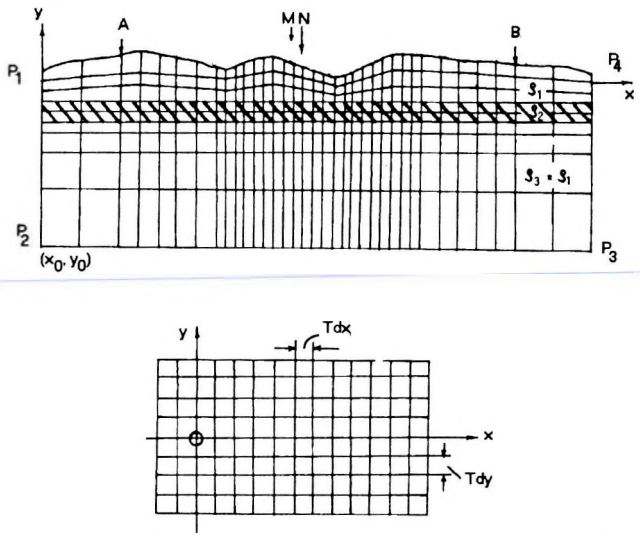


*Fig. 1.* Three-layer geoelectric model for finite-element method to compute two-dimensional terrain correction

*1. ábra.* Háromréteges geoelektromos modell kétdimenziós terén korrekció számításához

*Рис. 1.* Двухмерная трехслойная геоэлектрическая модель для расчета поправки за влияние рельефа методом конечных элементов

publications [e.g. HOLCOMBE, JIRACEK 1984, FOX et al. 1980 or PRIDMORE et al. 1981]. For the calculation of terrain effect along two-dimensional structure a special algorithm was used, the mathematical elements of which are presented in earlier works of the author [FRASHËRI 1987, FRASHËRI et al. 1984].

In accordance with this algorithm a program, ELTRON-3, in Fortran-77 programming language was developed. This algorithm is different from those of many other authors [FOX et al. 1980, HOLCOMBE, JIRACEK 1984, MUNDRY 1984, SCRIBA 1981, PRIDMORE et al. 1981, GYIMESI, SIMON 1989]. We use the ordinary variational problem for elliptic differential equations as described by AMES [1977] and ZIENKIEWICZ [1977]. During the tests carried out on a BULL DPS7 computer with models consisting of a thousand nodes, the computer time ranged from 5 minutes (for profiling) to 30 minutes (for soundings). Correction of the terrain effects [FRASHËRI et al. 1984] and construction of synthetic curves of the apparent resistivity with arbitrarily curved layer boundaries for both sounding and profiling [FRASHËRI 1987] were performed by this program.

In *Fig. 2* the correction of the terrain effects is presented when the relief is broken by a crest and a valley; the geological section has two half-layers divided by a vertical plane. Apparent resistivities, measured with fixed-source gradient and Schlumberger arrays, present minima over the crest and maxima in the valley, accompanied by smaller anomalies on both sides. After terrain correction, the profiles of the apparent resistivity assume their normal view.

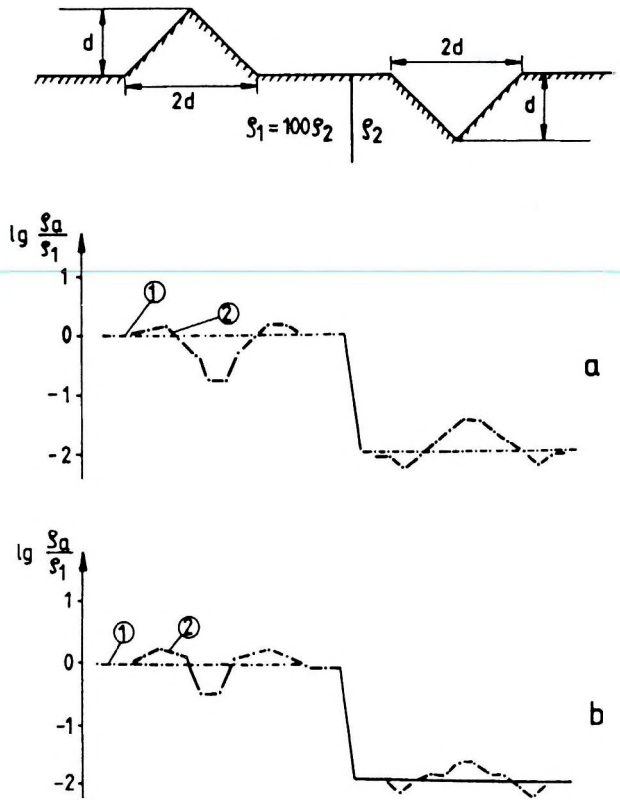


*Fig.* 2. Terrain corrections of resistivity profiling over a vertical contact, computed with ELTRON-3 program. a—fixed-source gradient array (MN=Δx=1/50 AB); b—on-line Schlumberger array (AB=6Δx=6 MN) 1—corrected curve; 2 —curve with terrain effects

*2. ábra.* Az ELTRON-3 programmal számított terrén korrekció értékek függőleges határfelület feletti ellenállás szelvényezéshez. a—gradiens elrendezés (MN=Δx=1/50 AB); b—Schlumberger elrendezés (AB=6Δx=6 MN) 1—korrigált görbe; 2— terrén hatást tartalmazó görbe

*Рис. 2.* Поправка данных электрического профилирования над вертикальным контактом, расчитанная программой ELTRON-3. a– по установке срединных градиентов при MN=Δx=1/50 AB; b–для симметричной установки AB=6Δx=6 MN 1–поправленный график; 2–исходный график с влиянием рельефа

In *Fig. 3* synthetic AMNB soundings carried out on a mountain crest and over a valley formed in homogeneous half-space are presented. For the soundings carried out over the valley or on the top of the crest, curves with similar appearance to the two-layer curves are obtained, the right flanks ascending and descending respectively. The interpretation of these curves may lead to a fictious two-layer section. When the soundings are carried out at the border of the crest or the valley, the curves have other three-layer configurations of the types K and H, respectively.

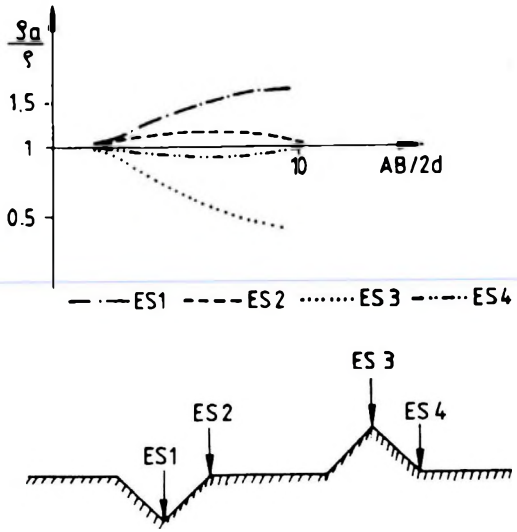


*Fig. 3.* Synthetic AMNB sounding curves over an isotropic homogeneous medium. Array parallel to the profile. ES1—in a valley; ES2—on the margin of a valley; ES3—at the top of a crest; ES4—on the margin of a crest

*3. ábra.* Szintetikus AMNB szondázási görbe izotróp homogén közeg felett. A terítés párhuzamos a szelvénnyel. ES1—egy völgyben; ES2—egy völgy szegélyén; ES3—egy hegygerinc tetején; ES4—egy gerinc szegélyén

*Рис. 3.* Теоретические кривые ВЭЗ над однородной изотропной средой. Точка ES1—размещена в долине; ES2—на крае долины; ES3—на хребте; ES4—на крае хребта

In *Fig. 4* apparent resistivity profiles of the fixed-source gradient array are presented over a section with 80 m level difference. Profile '1' is calculated in an analytical way with the above mentioned algorithm; profile '2' gained through physical modelling with electrical conductive paper is given for comparison. The shapes of these profiles are similar, although the absolute values of the apparent resistivity are different because the physical modelling does not possess the same conductivity as the mathematical model. The profiles reveal that the hills and the valleys cause anomalies of the apparent resistivity which amounts to some thousand ohmm above a medium of 1000 Ωm resistivity.

In all cases shown above, in the 2-D geoelectrical models the current sources A and B are point sources. All the soundings and the profilings are carried out parallel with the profile drawn in the figures.

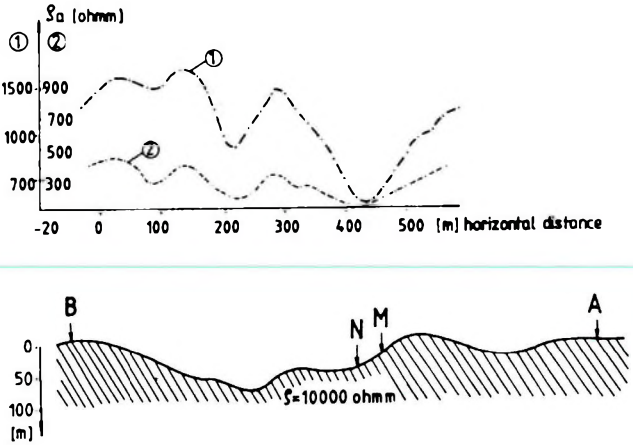


*Fig. 4.* Comparison of apparent resistivity profiles based on mathematical and physical modelling. Fixed source gradient array. 1—mathematical modelling; 2—physical modelling

*4. ábra.* Matematikai és fizikai modellezésen alapuló látszólagos ellenállás szelvényezés összehasonlítása. 1—matematikai modellezés; 2—fizikai modellezés

*Рис. 4.* Сопоставление графиков, полученных по данным математического и физического моделирования, для схемы срединных градиентов. 1—по данным математического моделирования; 2—по данным физического моделирования

## 3. Influence of buried and outcropped boundaries

Interfaces between rocks with different resistivity (for example limestones, flysch or halitic deposits in Albania) influence the scattering of the electric field; as a consequence the measured resistivity curve is deformed. The effect of outcropped, vertical contact was analysed by well-known authors [e.g. DAHNOV 1953]. Nomograms were constructed to correct the contact effect, when the position and the reflection coefficient of the contact are known. Evaluation of this influence is especially indispensable in the neighbourhood of resistive salt diapirs in Albania.

In *Fig. 5* a sounding observed near a salt diapir (1) is presented together with the corrected curve (2) for the influence of the vertical contact of the salts. The sounding is situated over flysch deposits with a resistivity of about 20 Ωm, covered by alluviums. The contact caused an increase in the resistivity of the second electric layer (flysch) to 50 Ωm and at the same time there are signs of a nonexistant third layer of high resistivity. After correction, these false phenomena could be avoided.

The study of the influence of more complicated boundary was possible by the ELTRON-3 program for 2-D models and ELTRONHA for 3-D models [FRASHËRI 1987]. In *Fig. 6* electric soundings are presented over two-layer models with a buried vertical contact. Interpreting the curves deformed by the

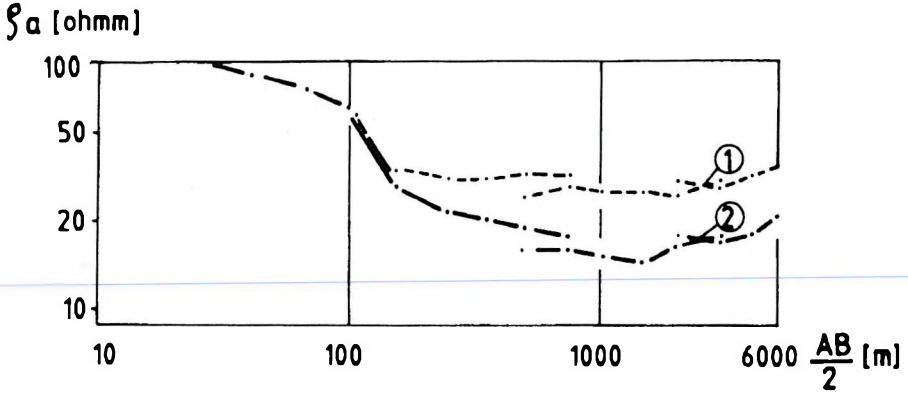


*Fig. 5.* Deformation of the apparent resistivity curve from the vertical contact and correction
1—uncorrected; 2—corrected

*5. ábra.* Látszólagos ellenállás görbe függőleges határfelület által okozott torzulása, és korrekció
1—nem korrigált görbe; 2—korrigált görbe

*Рис. 5.* Наблюденные искаженные и поправленные кривые при наличии вертикального контакта 1—наблюденная кривая; 2—поправленная кривая

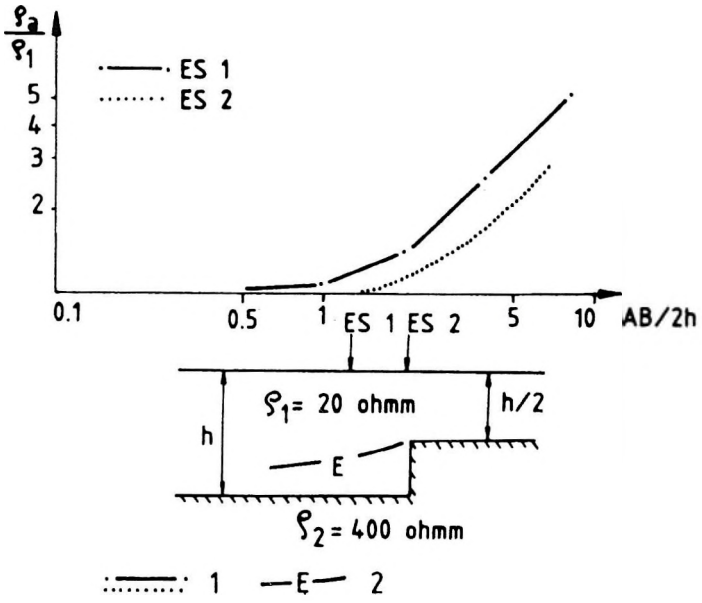


*Fig. 6.* Effect of a buried vertical contact. 1—sounding curves modelled with ELTRONHA program; 2—interpreted (false) boundary without the influence of vertical contact

*6. ábra.* Eltemetett függőleges határfelület hatása. 1—az ELTRONHA programmal modellezett szondázási görbe; 2—értelmezett (hamis) határfelület a függőleges érintkezés hatása nélkül

*Рис. 6.* Влияние флексуры. 1–кривая ВЭЗ, расчитанная по программе ELTRONHA; 2– ложный геоэлектрический горизонт, полученный при интерпретации непоправленной кривой

influence of the contact, the top of the basement is defined as being at a shallower depth than it really is. The impression of the existence of a right-hand structural flank is also created.

From the results of this modelling it can be concluded that precise determination of the thickness of the first layer can be carried out only when this thickness (i.e. the basement depth) is at least ten times smaller than the sounding distance from the vertical contact. For smaller distances the effect is not negliglible and the curves need to be corrected. In order to do this, we should previously know the position of the near-vertical contact. The presence of the vertical (even buried) contact of high resistivity causes a more distinct increase of the apparent resistivity in the right flank of the curve than in the case of horizontal layers. This peculiarity creates the possibility of detecting (in some cases) the vertical contact of high resistivity.

## 4. Influence of lateral resistivity changes in the geoelectrical horizons

Geophysical prospecting has revealed that there are facial changes, which in some regions of Albania are accompanied by great lateral resistivity changes. For example, the calcareous core of an anticline with limited (as small as 1-2 km) dimensions and the terrigenous deposits around it represents an extraordinarily great lateral change in the layer resistivity.

In order to study the influence of the lateral change of the layer resistivity for this type of anticline, we modelled — exploiting the ELTRON-3 program — the case when the structure is slightly wider than its depth (see *Fig. 7*). Analysing the calculated curves, it is obvious that the side effects of the resistive basement is felt even at long distances from the edge of the horst, and it is expressed by an increase in the apparent resistivity.

Two-layer curves of the apparent resistivity do not have regular configuration, they are much more similiar to the curves of inclined layers with considerable dip angle to the side vertical contact. If the electric soundings are carried out with a shorter array than is needed for the whole curve, only the beginning of the upward left flank will be obtained. Observing these short curves it can be supposed that the top of the limestone becomes deeper the further it is from the horst centre, belonging to a wide anticlinal structure. Over structures that have comparable dimensions and layering depth, the apparent resistivity is reduced as a consequence of current deviation because the electric current flows alongside the structure. This causes the top of the structure to appear as if it is at a greater depth than it really is.

Sounding carried out in grabens filled with conductive overburden and bordered by rocks of high resistivity (e.g. limestone), displays a deformed curve as well, when the width of the graben is smaller then the length of the electrical sounding array. To avoid the influence of the above analysed phenomenon and the misleading interpretation the following measures should be taken:

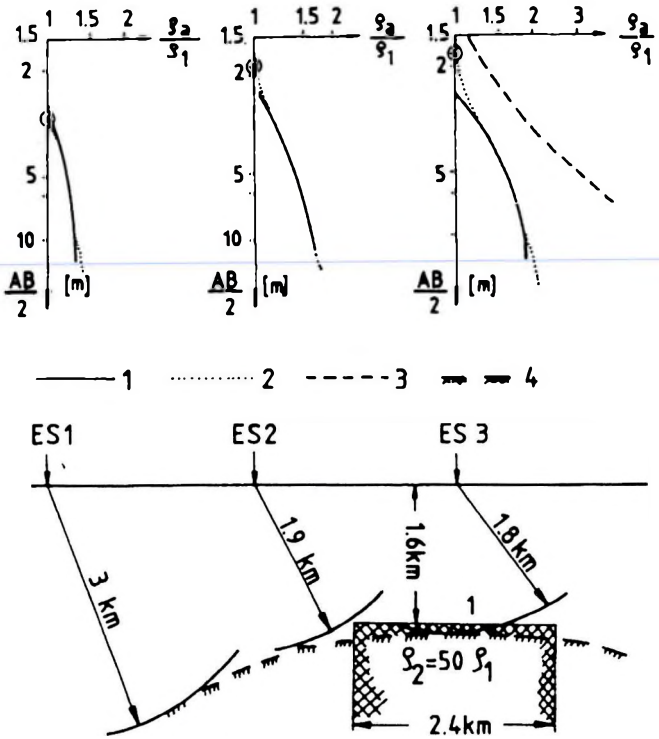


*Fig. 7.* Apparent resistivity curves placed across a horst. 1—synthetic curves computed with ELTRON-3 program; 2—analytical curves that fit to the synthetic curves; 3—analytical curve assuming the horst to be horizontally infinite; 4—geoelectric horizon after interpretation which does not consider the horst limited in the horizontal direction

*7. ábra.* Látszólagos ellenállás görbék egy sasbércen keresztül. 1—az ELTRON-3 programmal számított szintetikus görbék; 2—a szintetikus görbére illesztendő analitikus görbék; 3—analitikus görbék a sasbérc oldalirányú végtelen kiterjedését feltételezve; 4— geoelektromos szint értelmezés után, nem véve figyelembe a sasbérc korlátozott oldalirányú kiterjedését

*Рис. 7.* Кривые ВЭЗ по профилю, расположенному вкрест горста.1—Синтетические кривые, расчитанные по программе ELTRON-3; 2—Теоретические кривые, совпадающие с синтетическими; 3—теоретические кривые при горизонтальном положении кровли бесконечного горста; 4—Ложный геоэлектрический горизонт, полученный при интерпретации без учета влияния ограниченности горста в боковом направлении

— field and regular surveys should be carried out, to detect as clearly and surely as possible the structures. When interpreting the soundings, structures may turn out to be different in form and dimensions from the surrounding structures and may not correspond to the recognized tectonics of the region. In such cases the side effects of the soundings should be thoroughly studied;

— study of the structural form should be carried out together with a study of the lateral resistivity changes in the layers constituting the section over the geoelectric horizon as well as the horizon itself;
— sounding should be carried out with long array, so that the sounding curve to be as complete as possible; this allows us to carry out some sort of classification of the distortion effects;
— interpretation of the curves carried out in the regions of complicated geology should not be carried out solely by comparing the theoretical models for horizontal layers. Interpretation should begin with a comparison of the curve of the parametric soundings on boreholes with the synthetic curves calculated from the data of electrical well logging. These synthetic curves should be computed for simple models with horizontal layers as well as for the supposed geoelectrical structures in the region applying the ELTRON-3 program.

## 5. Conclusions

The apparent resistivity values measured during electric soundings in geologically disturbed (tectonized, folded, mountainous) zones reveal the influence of lateral contacts, gradual lateral changes of resistivity, and of the rugged terrain. The influences can add up to 50% of the resistivity values. Hence the curves of the electrical sounding are deformed, thereby influencing the geoelectrical interpretation as well. To analyse the above mentioned effects it is necessary to implement a regular grid of soundings and it is advisable to keep the length of the arrays sufficiently long. Correction of the apparent resistivity values is needed. The finite-element method is suitable for computing the apparent resistivity of soundings or profilings in a heterogeneous environment. The programs ELTRON-3 for 2-D models and ELTRONHA for 3-D models can be utilized for this purpose. These models are of great value for qualitative interpretation.

To avoid the terrain effects, the effects of the buried vertical contact, and the lateral structures parallel to the array, it is essential to use 3-D finite-element modelling.

## REFERENCES

AMES W. F. 1977: Numerical methods for partial differential equations. 2nd ed. New York, Academic Press Inc.

DAHNOV V. N. 1953: Electrical Prospecting for oil and gas reservoirs. (in Russian) Moscow, Gostgeoltehizdat

GYIMESI M., SIMON A. 1989: Approximate calculation of the electric field of a buried DC source using the finite element method for several 2D models. *In*: Abstract and papers, 34th Int. Geoph. Symp., Budapest

FOX R. C., HOHMANN G. W., KILLPACK T. J., RIJO L. 1980: Topographic effects in resistivity and induced polarization surveys. Geophysics, **45**, 1, pp. 75-93

FRASHËRI A., TOLE Dh., FRASHËRI N. 1984: An algorithm for the study of the electrical field scattering with the assistance of finite elements, on media divided by curved boundaries. (In Albanian) Buletini i Shkencave te Natyres No. 1, pp. 22-31

FRASHËRI A. 1987: Investigation of electrical field scattering through heterogeneous geological media. (In Albanian) Ph.D. thesis, University of Tirana

HOLCOMBE H. T., JIRACEK G. R. 1984: Three-dimensional terrain corrections in resistivity surveys. Geophysics, **49**, 4, pp. 439-452

KOEFOED O. 1979: Geosounding Principles 1. Resistivity sounding measurements. Amsterdam-Oxford-New York, Elsevier, 276 p.

MUNDRY E. 1984: Geoelectrical model calculations for two-dimensional resistivity distributions. Geophysical Prospecting, **32**, 1, pp. 124-131

SCRIBA H. 1981: Computation of the electric potential in three-dimensional structures. Geophysical Prospecting **29**, 5, pp. 790-802

PRIDMORE D. F., HOHMANN G.W., WARD S. H., SILL W. R. 1981: An investigation of finite-element modeling for electrical and electromagnetic data in three dimensions. Geophysics **46**, 7, pp. 1009-1024

ZIENKIEWICZ O. C. 1977: The Finite Element Method. McGraw-Hill Book Co., London-New York, 787 p.

## ELEKTROMOS SZONDÁZÁS ÉS SZELVÉNYEZÉS ÉRTELMEZÉSI PROBLÉMÁI BONYOLULT FÖLDTANI SZERKEZTŰ ÉS EGYENETLEN FELSZÍNŰ TERÜLETEKEN

Alfred FRASHËRI

Komplikált geológiájú és egyenetlen felszínű területeken (pl. Albanidák gyűrt hegyláncai) végzett elektromos szondázások az elektromos tér szóródását mutatták. A bonyolult geoelektromos közeg jellemzői az ellenállás oldalirányú változásai, a geológiai szerkezetek véges kiterjedése, számos, egymáshoz közel fekvő szerkezet és az egyenetlen felszín.

Mivel az elektromostér szóródása torzítja a látszólagos ellenállás értékeket, az ellenállás görbék kiértékelése e jelenség figyelembevétele és hatásainak korrigálása nélkül megbízhatatlan kép kialakulásához vezethet. Ezért egyenáram elektromos terének szóródását vizsgáltuk heterogén közegben, törött határfelületek és egyenetlen terepviszonyok mellett. A potenciál válaszokat kváziharmonikus potenciálegyenlet (két- és háromdimenziós) segítségével határoztuk meg, Neumann-féle határfeltételek figyelembevételével. A kváziharmonikus egyenlet trapezoid alakzatra való megoldásához az alsó féltérben a megfelelő variációs problémával helyettesítettük azt. Így a véges elemes módszerrel előállítható a megoldás, az elektromos tér szóródásának egy közelítő leírását biztosítva. Két számítógépes programot készítettünk Fortran nyelven, kétdimenziós és háromdimenziós modellezéshez.

Bemutatjuk néhány geoelektromos modell eredményét. A modellekben az elektromos szondázásokat különböző típusú kőzetek határfelületei, vagy sasbércek és árkok fölé helyeztük. A programok különböző hatások korrekcióinak végrehajtására is szolgálnak, beleértve a terrén korrekciót is.

# ПРОБЛЕМЫ ИНТЕРПРЕТАЦИИ ДАННЫХ ЭЛЕКТРИЧЕСКОГО ЗОНДИРОВАНИЯ И ПРОФИЛИРОВАНИЯ НА УЧАСТКАХ, ХАРАКТЕРИЗУЮЩИХСЯ СЛОЖНЫМ ГЕОЛОГИЧЕСКИМ СТРОЕНИЕМ И НЕРОВНОСТЬЮ РЕЛЬЕФА

Альфред ФРАШЕРИ

Вертикальные электрические зондирования, проведенные в горных районах при сложном геологическом строении (как складчатый пояс Албании), показали сильно искаженное геологическое поле. Характерными особенностями такой геологической среды являются: боковые изменения удельного электрического сопротивления, ограниченные размеры геологических объектов, наличие нескольких структурных элементов друг над другом и горный рельеф.

Аномальное распределение электрического поля искажает значение кажущегося сопротивления. Традиционная обработка кривых ВЭЗ без учета влияния выше отмеченных особенностей приводит к ложной интерпретации данных. Поэтому изучалось распределение поля постоянного тока в неоднородной среде с кривыми границами раздела в условиях горного рельефа.

Потенциал электрического поля вычислялся для двухмерных и трехмерных моделей путем решения квази-гармонического уравнения с граничными условиями типа Наймана. Решение квази-гармонического уравнения для трапезоидальной зоны в нижнем полупространстве было замещано вариационной проблемой, которая решалась методом конечных элементов, дающим приближенное представление о распределении электрического поля. Для расчетов составлены две программы на языке Фортран для двух- и трехмерных моделей соответственно.

Показаны результаты расчетов для некоторых геоэлектрических моделей. Расчеты выполнены для вертикального электрического зондирования на поверхности полупространства с кривыми границами раздела типа контакта геологических образований, флексуры, над горстом и грабеном. Эти же программы были применены для вычисления поправки за разные влияния, включая и влияние рельефа местности.

# EÖTVÖS L. GEOPHYSICAL INSTITUTE OF HUNGARY

## THE OLDEST INSTITUTION FOR APPLIED GEOPHYSICS OFFERS THE LATEST ACHIEVEMENTS FOR GROUND-WATER PROSPECTING and ENVIRONMENTAL PROTECTION

The most often occurring demands:

- local geophysical measurements for the water supply of small communities by a few wells
- regional geophysical mapping to determine hydrological conditions for irrigation, regional agricultural development,
- large-scale exploration for the water supply of towns, extended areas i.e. regional waterworks,
- determination of bank storage of river terraces, planning of bank filtered well systems,
- thermal water exploration for use as an energy source, agricultural use or community utilization,
- cold and warm karst water prospecting,
- water engineering problems, water construction works

*The Maxi-Probe electromagnetic sounding and mapping system – produced under licence by Geoprobe Ltd. Canada – is an ideal tool for shallow depths, especially in areas where seismic results are poor or unobtainable*

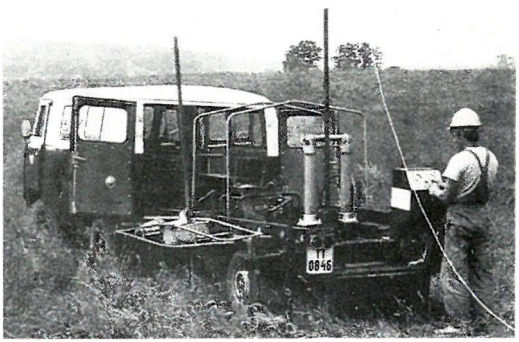

*ELGI has a vast experience in solving problems of environmental protection such as control of surface waters, reservoir construction, industrial and communal waste disposal, protection of surface and ground water etc. ELGI's penetrologger provides in-situ information – up to a maximum depth of 30 m – on the strength, sand/shale ratio and density without costly drilling.*

*Field work with ELGI's 24-channel portable seismograph*

**ELGI offers contracts with co-operating partners to participate in the whole complex process of exploration–drilling–production.**

**For further information ask for our booklets on instruments and applications. Let us know your problem and we will select the appropriate method and the best instrument for your purpose.**

*Our address: ELGI POB 35. Budapest, H–1440. HUNGARY*
*Telex: 22-6194 elgi h*

## INVITATION

The Association of Hungarian Geophysicists decided at its annual meeting to establish the "Foundation for Hungarian Geophysicists" and elected its first Advisory Board for 3 years. The foundation has been started with a moderate initial capital of 300 000 HUF, which has by now increased to more than 3 million and it is open for everybody.

The aim of the foundation is to help Hungarian geophysicists. There are two main target groups whose application for grants will be accepted with preference: young geophysicists needing assistance (travels, participation at conferences, publications,post-graduate education etc.) at the beginning of their professional life as well as retired and unemployed colleagues whose economic and social position became especially unfavourable.

The nine members of the Advisory Board invite everybody to join this foundation; donations should be communicated with the Board. Organisations and persons donating sums exceeding the initial capital will have the opportunity to delegate representatives into the Board. Detailed information is available at the following address:

Advisory Board of the
"Foundation for Hungarian Geophysicists"
H–1371 Budapest, P.O.B. 431
Budapest, I., Fő u. 68.
Telephone 201-2011/590
Telex 22-4343
Telefax 156-1215